AD-A072 998 ARMY COMMUNICATIONS RESEARCH AND DEVELOPMENT COMMAND --ETC F/G 20/3
SCATTERING FROM PERIODIC SURFACES WITH SINUSOIDAL HEIGHT PROFIL--ETC(U)
JUN 79 G M WHITMAN, F SCHWERING

UNCLASSIFIED CORADCOM-79-5 NL

1 OF 1
ADA 072998

END
DATE FILMED
9-79
DDC

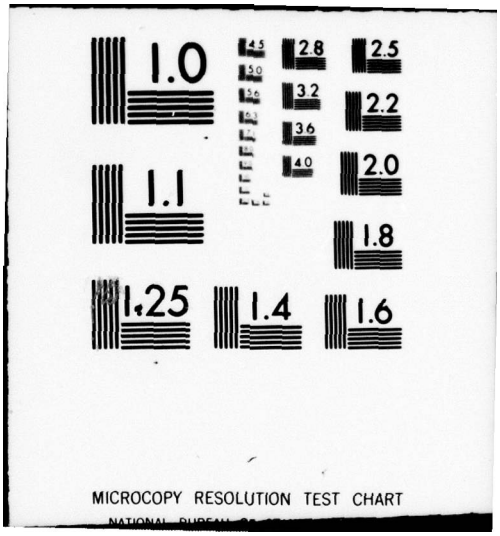
1.0
1.1
1.25
1.4
1.6
1.8
2.0
2.2
2.5
2.8
3.2
3.6
4.0
4.5
5.0
5.6
MICROCOPY RESOLUTION TEST CHART

LEVEL II

12

B.S.

RESEARCH AND DEVELOPMENT TECHNICAL REPORT
CORADCOM-79-5

AD A072698

SCATTERING FROM PERIODIC SURFACES WITH SINUSOIDAL HEIGHT PROFILE - A THEORETICAL APPROACH - PART II: NUMERICAL EVALUATION

G. M. Whitman
F. Schwering

COMMUNICATIONS SYSTEMS CENTER

June 1979

CORADCOM
US ARMY COMMUNICATION RESEARCH & DEVELOPMENT COMMAND
FORT MONMOUTH, NEW JERSEY 07703

410489

NOTICES

Disclaimers

The citation of trade names and names of manufacturers in this report is not to be construed as official Government indorsement or approval of commercial products or services referenced herein.

Disposition

Destroy this report when it is no longer needed. Do not return it to the originator.

UNCLASSIFIED

SECURITY CLASSIFICATION OF THIS PAGE (When Data Entered)

REPORT DOCUMENTATION PAGE	READ INSTRUCTIONS BEFORE COMPLETING FORM
1. REPORT NUMBER: CORADCOM-79-5 (14)	2. GOVT ACCESSION NO. / 3. RECIPIENT'S CATALOG NUMBER (9)
4. TITLE (and Subtitle): Scattering from Periodic Surfaces with Sinusoidal Height Profile - A Theoretical Approach - Part II. Numerical Evaluation. (6) AD72984	5. TYPE OF REPORT & PERIOD COVERED: Final Report, 1 July 1973 — 30 June 1976
	6. PERFORMING ORG. REPORT NUMBER
7. AUTHOR(s): G. M. Whitman, F. Schwering (10)	8. CONTRACT OR GRANT NUMBER(s): DAHC04-72-A-0001 Task Order 74-407
9. PERFORMING ORGANIZATION NAME AND ADDRESS: CENCOMS, DRDCO-COM-RM-4, US Army Communications R&D Command, Fort Monmouth, N.J. 07703	10. PROGRAM ELEMENT, PROJECT, TASK AREA & WORK UNIT NUMBERS: 1L1 611102.H48.H2.11.01
11. CONTROLLING OFFICE NAME AND ADDRESS: CENCOMS/CORADCOM, Fort Monmouth, N.J. 07703	12. REPORT DATE: (11) June 1979
	13. NUMBER OF PAGES: 62 (12) 70 p.
14. MONITORING AGENCY NAME & ADDRESS(if different from Controlling Office)	15. SECURITY CLASS. (of this report): Unclassified
	15a. DECLASSIFICATION/DOWNGRADING SCHEDULE

16. DISTRIBUTION STATEMENT (of this Report)

APPROVED FOR PUBLIC RELEASE; DISTRIBUTION UNLIMITED

17. DISTRIBUTION STATEMENT (of the abstract entered in Block 20, if different from Report)

18. SUPPLEMENTARY NOTES

19. KEY WORDS (Continue on reverse side if necessary and identify by block number)

Periodic surface scattering;
Sinusoidal height profile;
Plane wave scattering;
Space harmonics;
Extended boundary condition;
Rayleigh type Wood anomalies

20. ABSTRACT (Continue on reverse side if necessary and identify by block number)

A theory of scattering by periodic metal surfaces is presented which utilizes the physical optics approximation to determine the current distribution in the metal surface in first order, but modifies this approximate distribution by multiplication with a Fourier series whose fundamental period is that of the surface profile (Floquet's theorem). The coefficients of the Fourier series are determined from the extended boundary condition that the field radiated by the current distribution into the lower (shielded) half-space must cancel the primary plane wave in this space range. The theory (Cont'd)

DD FORM 1 JAN 73 1473 EDITION OF 1 NOV 65 IS OBSOLETE

UNCLASSIFIED

SECURITY CLASSIFICATION OF THIS PAGE (When Data Entered)

410 489

20. ABSTRACT (Cont'd)

reduces the scatter problem to the familar task of solving a linear system. For certain basic topics of surface profiles, including the sinusoidal profile considered here, the coefficients of the linear system are obtained as closed form expressions in well-known functions (Bessel functions for sinusodial profiles and exponential functions for piece-wise linear profiles). The theory is thus amenable to efficient computer evaluation.

In part I of this report the theory is presented in detail; part II reports on numerical results obtained by computer evaluation of the theory.

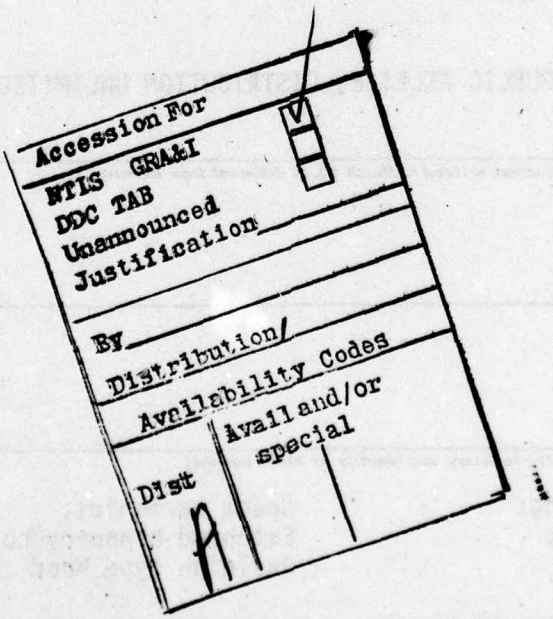

TABLE OF CONTENTS

	PAGE
1. INTRODUCTION	1
2. CURRENT DISTRIBUTION	2
3. SPACE HARMONICS	
a. Power vs. Incidence Angle	3
b. Anomalies	3
c. Dependence on Surface Depth	5
4. ACCURACY CHECK	6
a. Conservation of Power	6
b. Reciprocity Theorem	7
c. Limitations of Method	8
5. COMPARISON WITH EXISTING METHODS	9
6. ACKNOWLEDGEMENTS	11

LIST OF FIGURES

Fig. 1. Sinusoidal metal surface illuminated by plane wave. Coordinates and geometrical parameters used in analysis of scatter problem. 12

Fig. 2a. Modulus of current distribution over one period of sinusoidal metal surface illuminated by TE-polarized plane wave incident at $\theta = 0.01°$. 13

Fig. 2b. Phase of current distribution over one period of sinusoidal metal surface illuminated by TE-polarized plane wave incident at $\theta = 0.01°$. 14

Fig. 3a. Modulus of current distribution over one period of sinusoidal metal surface illuminated by TM-polarized plane wave incident at $\theta = 0.01°$. 15

Fig. 3b. Phase of current distribution over one period of sinusoidal metal surface illuminated by TM-polarized plane wave incident at $\theta = 0.01°$. 16

Fig. 4a. Modulus of current distribution over one period of sinusoidal metal surface illuminated by TE-polarized plane wave incident at $\theta = 30°$. 17

Fig. 4b. Phase of current distribution over one period of sinusoidal metal surface illuminated by TE-polarized plane wave incident at $\theta = 30°$. 18

Fig. 5a. Modulus of current distribution over one period of sinusoidal metal surface illuminated by TM-polarized plane wave incident at $\theta = 30°$. 19

Fig. 5b. Phase of current distribution over one period of sinusoidal metal surface illuminated by TM-polarized plane wave incident at $\theta = 30°$. 20

Fig. 6a. Modulus of current distribution over one period of sinusoidal metal surface illuminated by TE-polarized plane wave incident at $\theta = 60°$. 21

TABLE OF CONTENTS (cont'd.)

	PAGE
Fig. 6b. Phase of current distribution over one period of sinusoidal metal surface illuminated by TE-polarized plane wave incident at $\theta = 60°$.	22
Fig. 7a. Modulus of current distribution over one period of sinusoidal metal surface illuminated by TM-polarized plane wave incident at $\theta = 60°$.	23
Fig. 7b. Phase of current distribution over one period of sinusoidal metal surface illuminated by TM-polarized plane wave incident at $\theta = 60°$.	24
Fig. 8a. Modulus of current distirbution over one period of sinusoidal metal surface illuminated by TE-polarized plane wave incident at $\theta = 85^0$.	25
Fig. 8b. Phase of current distribution over one period of sinusoidal metal surface illuminated by TE-polarized plane wave incident at $\theta = 85^0$.	26
Fig. 9a. Modulus of current distribution over one period of sinusoidal metal surface illuminated by TM-polarized plane wave incident at $\theta = 85^0$.	27
Fig. 9b. Phase of current distribution over one period of sinusoidal metal surface illuminated by TE-polarized plane wave incident at $\theta = 85^0$.	28
Fig. 10. Direction angles θ_m of propagating space harmonics of scatter field vs. incidence angle θ of primary plane wave ($d/\lambda = 2.5$).	29
Fig. 11a. Powers P_m of propagating space harmonics vs. incidence angle θ of primary wave. Spectral orders: m = +2,+1,0. Polarization:TE. Surface parameters: $d/\lambda = 2.5$, $h/\lambda = 0.375$.	30
Fig. 11b. Powers P_m of propagating space harmonics vs. incidence angle θ of primary wave. Spectral orders: m = -1, -2, -3, -4. Polarization:TE. Surface parameters: $d/\lambda = 2.5$, $h/\lambda = 0.375$.	31
Fig. 12a. Powers P_m of propagating space harmonics vs. incidence angle θ of primary wave. Spectral orders: m = +2,+1,0. Polarization:TM. Surface parameters: $d/\lambda = 2.5$, $h/\lambda = 0.375$.	32
Fig. 12b. Powers P_m of propagating space harmonics vs. incidence angle θ of primary wave. Spectral orders: m = -1, -2, -3, -4. Polarization: TM. Surface parameters: $d/\lambda = 2.5$, $h/\lambda = 0.375$.	33
Fig. 13. Direction angles θ_m of propagating space harmonics of scatter field vs. incidence angle θ of primary plane wave ($d/\lambda = 1.3$).	34
Fig. 14a. Powers P_m of propagating space harmonics vs. incidence angle θ of primary wave. Spectral orders: m = +1,0. Polarization:TE. Surface parameters: $d/\lambda = 1.3$, $h/\lambda = 0.1333$.	35
Fig. 14b. Powers P_m of propagating space harmonics vs. incidence angle θ of primary wave. Spectral orders: m = -1, -2. Polarization:TE. Surface parameters: $d/\lambda = 1.3$, $h/\lambda = 0.1333$.	36
Fig. 15a. Powers P_m of propagating space harmonics vs. incidence angle θ of primary wave. Spectral orders: m = + 1,0. Polarization:TM. Surface parameters: $d/\lambda = 1.3$, $h/\lambda = 0.1333$.	37
Fig. 15b. Powers P_m of propagating space harmonics vs. incidence angle θ of primary wave. Spectral orders: m = -1, -2. Polarization:TM. Surface parameters: $d/\lambda = 1.3$, $h/\lambda = 0.1333$.	38
Fig. 16a. Powers P_m of propagating space harmonics as function of groove depth h/λ (TE-polarization, $\theta = 30°$, $d/\lambda = 2.5$).	39

TABLE OF CONTENTS (cont'd.)

PAGE

Fig. 16b. Powers P_m of propagating space harmonics as function of groove depth h/λ (TM-polarization, $\theta = 30°$, $d/\lambda = 2.5$). 40

Fig. 17a. Powers P_m of propagating space harmonics as function of groove depth h/λ (TE-polarization, $\theta = 60°$, $d/\lambda = 2.5$). 41

Fig. 17b. Powers P_m of propagating space harmonics vs. function of groove depth h/λ (TM-polarization, $\theta = 60°$, $d/\lambda = 2.5$). 42

Fig. 18a. Powers P_m of propagating space harmonics vs. function of groove depth h/λ (TE-polarization, $\theta = 85°$, $d/\lambda = 2.5$). 43

Fig. 18b. Powers P_m of propagating space harmonics vs. function of groove depth h/λ (TM-polarization, $\theta = 85°$, $d/\lambda = 2.5$). 44

Fig. 19a. Powers P_m of propagating space harmonics vs. function of groove depth h/λ (TE-polarizatiohn, $\theta = 22.62°$ (Brewster Angle)), $d/\lambda = 1.3$). 45

Fig. 19b. Powers P_m of propagating space harmonics vs. function of groove depth h/λ (TM-polarization, $\theta = 22.62°$ (Brewster Angle), $d/\lambda = 1.3$). 46

LIST OF TABLES:

Table 1: Accuracy check using power criterion. Surface parameters: $d/\lambda = 2.5$, $h/\lambda = 0.375$. 47

Table 2: Accuracy check using power criterion. Surface parameters: $d/\lambda = 1.3$, $h/\lambda = 0.1333$. 48

Table 3: Accuracy check using reciprocity criterion. Surface parameters: $d/\lambda = 2.5$, $h/\lambda = 0.375$. Polarization: TE 49

Table 4: Accuracy check using reciprocity criterion. Surface parameters: $d/\lambda = 2.5$, $h/\lambda = 0.375$. Polarization: TM 50

Table 5: Dependence of power errors ε_{TE} and ε_{TM} on surface depth. Surface period: $d/\lambda = 2.5$. Incidence angle: $\Theta = 30°$ 51

Table 6: Dependence of power errors ε_{TE} and ε_{TM} on surface depth. Surface period: $d/\lambda = 1.3$. Incidence angle $\Theta = 22.62°$ (Brewster angle) 52

Table 7a. Comparison of approaches: Complex amplitudes of space harmonics. (TE - polarization; $d/\lambda = 0.2$, $h/\lambda = 0.1$) 53

Table 7b: Comparison of approaches: Complex amplitudes of space harmonics. (TE - polarization; $d/\lambda = 1.9$, $h/\lambda = 0.25$; $\Theta = 0°$) 53

TABLE OF CONTENTS (cont'd.)

PAGE

Table 7c: Comparison of approaches: Complex amplitudes of space harmonics (TE - Polarization; $d/\lambda = 0.4$, $h/\lambda = 0.2$) 54

Table 7d: Comparison of approaches: Complex amplitudes of space harmonics (TE - polarization; $d/\lambda = 0.2$, $h/\lambda = 0.03$; $\theta = 0^o$) 54

Table 8a: Comparison of approaches: Complex amplitudes of space harmonics (TM - polarization; $d/\lambda = 0.2$, $h/\lambda = 0.1$) 55

Table 8b: Comparison of approaches: Complex amplitudes of space harmonics (TM - polarization; $d/\lambda = 1.9$, $h/\lambda = 0.25$; $\theta = 0^o$) 55

Table 8c: Comparison of approaches: Complex amplitudes of space harmonics (TM - polarization; $d/\lambda = 0.4$, $h/\lambda = 0.2$) 56

Table 8d: Comparison of approaches: Complex amplitudes of space harmonics (TM - polarization; $d/\lambda = 0.2$, $h/\lambda = 0.03$; $\theta = 0^o$) 56

Table 9: Comparison of approaches: Total scatter power and relative power error (TE - polarization) 57

Table 10: Comparison of approaches: Total scatter power and relative power error (TM - polarization) 58

Table 11a: Scattering form surfaces of large surface period: Comparison of W-S theory and physical optics approximation. 59
Surface parameters: $d/\lambda = 10$, $h/\lambda = 0.5$
Angle of incidence: $\theta = 15^o$

Table 11b: Scattering from surfaces of large surface period: Comparison of W-S theory and physical optics approximation. 60
Surface parameters: $d/\lambda = 10$, $h/\lambda = 0.5$
Angle of incidence: $\theta = 45^o$

Table 11c: Scattering from surfaces of large surface period: Comparison of W-S theory and physical optics approximation. 61
Surface parameters: $d/\lambda = 10$, $h/\lambda = 0.5$
Angle of incidence: $\theta = 75^o$

Table 11d: Scattering from surfaces of large surface period: Comparison of W-S theory and physical optics approximation. 62
Surface parameters: $d/\lambda = 10$, $h/\lambda = 0.5$
Angle of incidence: $\theta = 85^o$

SCATTERING BY PERIODIC SURFACES WITH SINUSOIDAL HEIGHT PROFILE-A THEORETICAL APPROACH

PART II: Numerical Evaluation

1. INTRODUCTION

In part I of this study, a theoretical approach to the problem of scattering by periodically corrugated metal surfaces is presented which is basically an extension of the physical optics approximation leading to a rigorous theory. The theory assumes the current distribution in the metal surface to be the physical optics current density modified by multiplication with a Fourier series whose fundamental period is equal to the period of the surfaces grooves (Floquet's theorem). The coefficients of the Fourier series are determined from the extended boundary condition which requires that the field radiated by the current distribution into the half-space below the metal surface cancel the incident field in this half-space. The method reduces the scatter problem to the familiar problem of solving a linear system. A particular advantage of this method is that for certain basic types of height profiles, including the sinusodial profile considered here, all matrix coefficients of the linear system reduce to closed form expressions of well-known functions. The theory is thus amenable to efficient computer evaluation.

A computer program has been written [1] and is operational. Numerical evaluations have been performed on the ECOM Burrough's B-5500 computer. Program outputs include the current distribution in the metal surface, the complex amplitudes of the plane wave spectrum (space harmonics representation) of the scatter field and an accuracy check based on conservation of power. This data has been computed for both TE-and TM-polarization, where TE and TM is understood with respect to the direction of the surface grooves.

The study has been performed in support of work on a practical problem, the polarization question of microwave landing systems. One of the aspects of this problem concerns scattering by large periodic metal surfaces, such as hangar doors, and the question whether the specular reflection coefficient of such surfaces can be significantly reduced by appropriate choice of polarization. The numerical results confirm experimental evidence

---

[1] The program is based on a formulation of the scatter problem using a Fourier representation of the current distribution in terms of sine and cosine functions rather than in terms of the complex exponential functions used in the theory presented in Part I. The latter representation leads to an analytically more elegant formulation and, therefore, has been preferred in presenting the theory.

[2] that horizontal polarization generally leads to substantially less specular reflection than vertical polarization, in particular in the interesting range of large angles of incidence (near grazing). It is implied here that the grooves of the periodic surface run in the vertical direction. In the limiting case of grazing incidence, the specular (amplitude) reflection coefficient of course approaches -1 for both polarizations.

Additional numerical data can be found in a preceeding summary report [3] which also discusses the case of circular polarization of the incident field. It is shown that this polarization is highly effective in suppressing higher order grating lobes having the same polarization (circular with the same sense of rotation) as the incident wave. Grazing lobes with the opposite sense of rotation are, in general, present with significant amplitudes. Such grazing lobes, however, would not be received by an airborne antenna polarized for optimum reception of the primary microwave beam.

Throughout Part II, the notation of Part I is used. To illustrate the scatter problem considered and the coordinates used, Fig. 1 of Part I is reproduced. As in Part I, it is assumed that the profile of the metal surface has the form

$$z = z\,(x) = h \sin(2\pi \frac{x}{d})$$

and that the primary field is a plane wave of (suppressed) time dependance $e^{i\omega t}$ incident in a direction parallel to the x,z-plane. The scatter problem for other directions of incidence can be mathematically reduced to this case.

2. CURRENT DISTRIBUTION

In Figures 2a through 9b, the current distribution over one period of the surface is plotted as a function of the lateral coordinate x. The curves apply to a surface profile with parameters $d/\lambda = 2.5$, $h/\lambda = 0.375$ and to incidence angles $\theta = 0^o$, 30^o, 60^o, and 85^o. The current distribution is periodic with the period d of the surface, except for a phase factor, $\exp(-ikx \sin\theta)$, determined by the incident plane wave (Floquet's theorem): see eqs. (15a) to (15c) of Part I. In the case of TE-polarization where the incident <u>electric</u> field strength has been assumed to have unit amplitude, the modulus of the current density is normalized by multiplication with $\sqrt{\mu_o/\varepsilon_o}$; in the case of the TM-polarization, the incident <u>magnetic</u> field strength has been assumed to have unit amplitude and no normalization is required.

---

[2] P. S. Demko, "Polarization/Multipath Study," Technical Memorandum VL-5-72, Avionics Laboratory, U. S. Army Electronics Command, Fort Monmouth, New Jersey, 1972.

[3] F. Schwering and G. Whitman, "A Theory of Scattering by Sinusoidal Metal Surfaces", Tech. Rept. ECOM-4496, U. S. Army Electronics Command, Fort Monmouth, N. J., May 1977.

In the valleys of the surface corrugations, i. e., in the range $-\frac{d}{2} \leq x \leq 0$, TE-polarization leads to appreciably smaller and less varying current densities than TM-polarization. This effect is pronounced in particular near normal incidence. Near grazing incidence, the surface currents for both TE - and TM - polarization are substantially reduced in magnitude over the entire metal surface.

3. SPACE HARMONICS

a. Power vs Incidence Angle

In Figures 11a through 12b and 14a through 15b, the powers P_m of the propagating space harmonics of the scatter field are plotted as functions of the incidence angle θ of the primary wave. Two surface profiles are considered; their parameters are $d/\lambda = 2.5$, $h/\lambda = 0.375$ and $d/\lambda = 1.3$, $h/\lambda = 0.1333$, respectively. P_m in these figures denotes the power transmitted by the m^{th} space harmonic through unit area of planes $z = \text{const.}$ assuming that the incident power per unit area is unity. Hence in the notation of Part I (see eqs. (20a) and (20b)):

$$P_m = \begin{cases} \left|E_m^{(1)}\right|^2 \dfrac{\cos\theta_m}{\cos\theta} & \text{for TE-polarization} \quad (1a) \\ \left|H_m^{(1)}\right|^2 \dfrac{\cos\theta_m}{\cos\theta} & \text{for TM-polarization} \quad (1b) \end{cases}$$

The direction angles θ_m of the propagating space harmonics versus incidence angle θ are shown in Figs. 10 and 13 for the two surface profiles considered. These curves apply to both TE-and TM-polarization.

Figures 11a to 12b and 14a to 15b show that in the range of large incidence angles ($\theta > 60^o$) the specular reflection coefficient (P_o) is significantly greater for TE-than for TM-polarization. This result is significant in the context of the polarization problem of microwave landing systems mentioned in the introduction. Thus undesired specular reflection of microwave beams from periodic structures, such as hanger doors at airports, can be substantially reduced by appropriate choice of polarization. The surface parameters used in the numerical evaluation approximate those of actual profiles.

b. Anomalies

The power distribution curves P_m vs θ, show Rayleigh-type Wood anomalies as discussed, for example, by Hessel and Oliner [4]. At angles of incidence, where one of the space harmonics is scattered into the direction of grazing and thus changes from being a propagating wave to being an evanescent one, or vice versa, the power distribution over the remaining space harmonics is radi-

---

[4] A. Hessel and A. A. Oliner, "A New Theory of Wood Anomalies on Optical Gratings", Applied Optics, 4, pp. 1275-1297, 1965.

cally altered and one or several spectral order may attain very high or near zero intensities. The incidence angles at which such anomalies occur are found from the relation for the propagation angles of the space harmonics (eq. (3a), Part I)

$$\sin \theta_m = \sin \theta + m \frac{\lambda}{d} \tag{2a}$$

by letting $\theta_m = \pm 90^o$. Thus

$$\theta = \theta_A = -\text{arc sin } (m \frac{\lambda}{d} \pm 1) \tag{2b}$$

These angles are indicated in Figs. 10 through 15b by small arrows. An additional anomaly occurs at $\theta = 90^o$ where the specular reflected wave is at grazing angles.

The anomalies are pronounced for TM-polarization (S-type anomalies) and weaker for TE-polarization (P-type anomalies). This can be explained by observing that - in particular, when $h<<\lambda$ - the electric field of a grazing TE wave is practically short circuited by the nearly plane conducting surface [5]. These results are in agreement with the experimentally well established fact that P-type anomalies require substantially deeper surface corrugation than S-type anomalies to become observable. For large d/λ- values, Rayleigh type anomalies tend to become less pronounced, which is probably due to the larger number of space harmonics involved in the redistribution of power. Note that for $d/\lambda = 2.5$ both anomalies are double anomalies [6] (two different space harmonics are at grazing angles simultaneously) so that a particularly strong effect can be expected. For $d/\lambda = 1.3$ only single anomalies occur.

A second type anomally expected to occur is of the "Brewster angle" type [7]; it can be characterized as a resonance between the incident wave and one of the space harmonics [5]. The condition for this type of resonance to take place is that

$$\theta = \theta_B = \text{arc sin } \{(n+\tfrac{1}{2}) \frac{\lambda}{d}\} , \tag{3}$$

---

[5] A. Hessel and J. Shmoys, "Computer Analysis of Propagation Reflection Phenomena", Polytechnic Institute of Brooklyn Scientific Report Contract Number AAB07-73-19-2716, August 1973.

[6] Double anomalies occur when d/λ is an integer or half integer; see eq. (2b).

[7] D. Y. Tseng, A. Hessel, and A. A. Oliner, "Scattering by a Multimode Corrugated Structure with Applications to P-type Wood Anomalies", Alta Frequenza, 38, 1968 Special Issue on the URSI Symposium on Electromagnetic Waves, Stresa, Italy.

but it also depends on the depth os the surface corrugations. It may occur for both TE- and TM-polarization but has been found to be more sensitively dependent on h in the latter case [8].

For $d/\lambda = 2.5$, conditions (2) and (3) yield the same values for θ_A and θ_B so that Rayleigh and Brewster angle anomalies may reinforce each other but are difficult to distinguish. For $d/\lambda = 1.3$ the Brewster angle condition yields

$$\theta_B = 22.52^o$$

Observe the decline of P_o (the specular reflected power) and the increase of P_{-1} near this angle in the case of TM-polarization; see Figs. 15a and 15b. Furthermore, Figs. 19a and 19b show that if the surface depth is appropriately chosen, i.e. $h/\lambda = 0.19$ for TM- and $h/\lambda = 0.27$ for TE- polarization, the specular reflected power becomes zero at this angle so that all power is propagated by the space harmonic of order $m = -1$. This means that the incident power is backscattered into the direction of arrival. From eqs. (2a) and (3) it can be seen that $\theta_{-1} = -\theta$ (backscatter condition) when the angle of arrival coinsides with the zero order Brewster angle, the situation considered in Figs. 19a and 19b.

c. Dependence on Surface Depth

Figs. 16a to 19b show the power propagated by the various space harmonics of the scatter field as functions of the depth of the surface grooves. Parameters are: $d/\lambda = 2.5$; $\theta = 30^o$, 60^o, 85^o and $d/\lambda = 1.3$; $\theta = 22.62^o$ (Brewster angle). Note that the groove depth is 2h rather than h, the parameter used in the figures.

For both polarizations, the dependence of P_m on h exhibits a basically oscillatory behavior, though TM-polarization tends to be more sensitive, in particular at angles of incidence near grazing; see Figs. 18a and 18b. These effects have been discussed by Zaki and Neureuther [9].

When the incidence wave is arriving at the Brewster angle, (Figs. 19a and 19b) the power of the specular reflected wave, $P_o(h)$, has zeros for both polarizations, as has been discussed above. However, in the TE- case, deeper

---

[8] See reference [5] on page 4.

[9] K. A. Zaki and A. R. Neureuther, "Scattering From a Perfectly Conducting Surface with Sinusodial Height Profile, TM-Polarization", IEEE Trans. Antennas and Prop., AP-19, pp. 747-751.

grooves are required to attain a zero than in the TM - case. Similarly, Figs. 16a and 16b show near-zeros occurring at $h/\lambda = 0.19$ for TM- and $h/\lambda = 0.26$ for TE-polarization[10]. These near- zeros apparently are due to the incidence angle, $\theta = 30^{\circ}$, being rather close to the Brewster angle at $\theta = 36.87^{\circ}$. Note that TM-polarization leads to a near - zero also at $\theta = 60^{\circ}$ though no Rayleigh-type or Brewster angle anomalies are expected in the vicinty of this angle. This near - zero may be attributed to a broad minimum of P_o (as a function of θ) in the range of large incidence angles; see Fig. 12a.

4. ACCURACY CHECK

Two criteria are used to check on the accuracy of computed data: conservation of power and reciprocity.

a. Conservation of Power

Since the metal surface is assumed perfectly conducting, the total scatter power, i.e., the accumulated power of all propagating space harmonics must equal the power of the incident wave. Hence, with eqs. (1a) and (1b)

$$\sum_m P_m \equiv \frac{1}{\cos\theta} \sum_m |E_m^{(1)}|^2 \cos\theta_m = 1 \tag{4a}$$

for TE-polarization and

$$\sum_m P_m \equiv \frac{1}{\cos\theta} \sum_m |H_m^{(1)}|^2 \cos\theta_m = 1 \tag{4b}$$

for TM-polarization. The summation is taken over the propagating spectral orders, i.e., over all integer m within the range

$$-\frac{d}{2}(1 + \sin\theta) < m < \frac{d}{2}(1 - \sin\theta).$$

See eq. (3b) of Part I.

In Tables 1 and 2, the relative power errors

$$\epsilon_{TE} = \frac{1}{\cos\theta} \sum_m |E_m^{(1)}|^2 \cos\theta_m - 1 \tag{3a}$$

and

$$\epsilon_{TM} = \frac{1}{\cos\theta_m} \sum_m |H_m^{(1)}|^2 \cos\theta_m - 1 \tag{3b}$$

---

[10] It is interesting to note that the groove depths h at which these zeros or near zeros occur are practically the same for $d/\lambda = 1.3$ and 2.5, the two cases considered here.

are listed as functions of θ for (1) $d/\lambda = 2.5$, $h/\lambda = 0.375$ and (2) $d/\lambda = 1.3$, $h/\lambda = 0.1333$, i.e., for the surface parameters considered in most of the figures. In addition to the power errors, the highest peaks of the current distributions in the metal surface are shown. Near the angles $\theta = \theta_A$, where Rayleigh-type Wood anomalies are expected to occur, smaller increments in θ are chosen in the tables to make effects apparent. As indicated in the figures, we have two Rayleigh wavelength angles for $d/\lambda = 2.5$ i.e.,

$$\theta_A = 11.54^\circ \text{ and } 36.87^\circ$$

However, since d/λ is a half integer, the associated anomalies are degenerate (double anomalies). For $d/\lambda = 1.3$ only single anomalies occur; the Rayleigh wavelength angles are

$$\theta_A = 13.34^\circ \text{ and } 32.58^\circ$$

The tables show that the accuracy attained with the new method [11] is excellent for parameters (2), and acceptable for parameters (1) apart from a small range of incidence angles near the second anomaly where the power error in the TM case reaches values in the order of 10%. In general, the accuracy for TE-polarization is higher than for TM-polarization, at most incidence angles by an order of magnitude. Note that passing an anomaly is usually accompanied by a sharp drop or increase in accuracy while the current amplitude tends to peak up near anomalies; see in particular, Table 1. The drastically increased current amplitude shown in this Table, at the second anomaly however, may not be real. In several instances it has been observed that a beginning loss of accuracy expresses itself more sensitively in a rapidly increasing amplitude of the current distribution rather than in an increasing violation of the power criterion, an effect which commences only later. As pointed out already in the discussion of Figs. 8a and 9a, the current amplitudes decline substantially for both polarizations as θ approaches 90°.

b. Reciprocity Theorem:

Consider two plane waves incident from directions θ^a and θ^b, respectively. If the first of these plane waves scatters a space harmonic of order m into the direction of the second wave such that [12] $\theta_m^a = -\theta^b$, then the second

---

[11] The power errors ϵ_{TE} and ϵ_{TM} depend, of course, on the degree to which the linear systems (18c) and (18d) of Part I are truncated in the numerical evaluation. The values listed in Tables 1 and 2 refer to systems of sizes 25 x 25 and 22 x 22, respectively.

[12] For explanation of the minus signs in the relations $\theta_m^a = -\theta^b$ and $\theta_m^b = -\theta^a$ we refer to Fig. 1. Incidence angles of the primary field are counted positive in the 2nd quadrant of the x,z-plane while the direction angles of the scatter field are counted positive in the 1st quadrant.

plane wave produces a space harmonic of the same order m propagating in the direction of the first incident wave, hence $\theta_m^b = -\theta^a$, and the complex amplitudes of the two space harmonics are related by:

$$\left(E_m^{(1)}\right)^a \cos\theta_m^a = \left(E_m^{(1)}\right)^b \cos\theta_m^b \qquad (4a)$$

for TE-polarization and

$$\left(H_m^{(1)}\right)^a \cos\theta_m^a = \left(H_m^{(1)}\right)^b \cos\theta_m^b \qquad (4b)$$

for TM-polarization. It is assumed here that the two incident waves have equal amplitude and phase. A specific advantage of the reciprocity relations is that they check amplitude and phase of individual space harmonics.

In Table 3 and 4 the results of a reciprocity check are shown; surface parameters are $d/\lambda = 2.5$, $h/\lambda = 0.375$. In the TE- case, relative amplitude errors are generally below 0.5% - larger errors are due to small amplitudes- and phase errors remain below 1^o. In the TM- case discrepancies are appreciably larger in conformance with a trend observed when applying the power criterion. In general, it has been found that when the power criteria is well satisfied the same is true for the reciprocity criterion, though specific power and reciprocity errors do not (and are not expected to) directly correlate.

c. Limitations of Method:

The accuracy of the computed results has been found to be sensitively dependent on the depth of the surface grooves i.e., on the parameter h/λ. The power and reciprocity criteria are excellently satisfied at small $h/\lambda < 0.1$ and well satisfied up to $h/\lambda \sim 0.5$. However when the surface depth approaches and is increased beyond one wavelength, the accuracy sooner or later breaks down (depending on d/λ and θ). This failure occurs for TE- and TM- polarization at approximately the same h/λ values. To demonstrate the decline of accuracy with increasing h, the power errors ϵ_{TE} and ϵ_{TM} encountered in computing the curves $P_m = P_m(h)$ of Figs. 16a, 16b and 19a, 19b are listed in Tables 5 and 6 as functions of h/λ. It has been found that the present program does not permit solution of the problem of declining accuracy by the obvious method of arbitrarily increasing the size of the linear systems, eqs. (18c) and (18d) of Part I, in the numerical evaluation. Up to now it has not been established whether the accuracy problem is due to inherent poor convergence of the linear systems at large h/λ or to a break down of subroutines employed in the computer program such as those for computing Bessel functions of complex arguments. Further work is required to answer this question and, if possible, to extend the h/λ range which can be handled by the program.

No limitations have been encountered with regard to admissible d/λ values. The accuracy as measured by the power criterion tends to increase with increasing d/λ which would be expected since the underlying method is basically an extension of the physical optics approximation.

5. COMPARISON WITH EXISTING METHODS

Tables 7a through 8d show a comparison of numerical values obtained by use of the new method (WS), the method by Tong and Senior (TS), and the physical optics approximation (PO). These tables have been taken directly from Tong and Senior [13] where only the values computed according to the new technique have been added [14]. Tables 9 and 10 compare the accuracy of these approaches in satisfying the power criterion.

The tables show that the WS and TS methods in general are in good agreement (apart form apparent sign errors in a number of cases), while the PO approximation leads to substantial errors as has been pointed out already by Tong and Senior. Such errors, however, are not unexpected since the periods d of the surfaces considered here do not satisfy the condition $d >> \lambda$ under which application of the PO approximtion would be justified. Taking shadow effects into account appears to increase, rather than decrease errors at the small d/λ ratios considered here. Tables 9 and 10 show that the accuracy of the WS method in general exceeds that of the TS method though improvements are not dramatic. There are exceptions; for example, for $d/\lambda = 0.4$, $h/\lambda = 0.2$, $\theta = 0^o$, the TS method satisfied the power criterion with smaller error than the WS method. On the other hand, for $d/\lambda = 0.2$, $h/\lambda = 0.1$, $\theta = 60^o$, the WS method exceeds the accuracy obtained with the TS method by an order of magnitude. For a comparison of the WS program with the program developed by Zaki and Neureuther see reference [3].

Tables 11a through 11d test the accuracy of the PO approximation in the case of a surface satisfying the condition $d >> \lambda$. Parameters are

$$\frac{d}{\lambda} = 10; \quad \frac{h}{\lambda} = 0.5; \quad \theta = 15^o, 45^o, 75^o, \text{ and } 85^o.$$

Listed are the power densities P_m of the propagating space harmonics computed according to the WS and PO[15] methods, respectively. For $\theta = 75^o$ and

---

[13] T. C-H. Tong and T. B. A. Senior, "Scattering Electromagnetic Waves by a Periodic Surface with Arbitrary Profile", Scientific Report AFCRL-72-0258, April 1972, prepared by the University of Michigan, Radiation Laboratory.

[14] Tong and Senior assume a cos-profile of the metal surface; the present theory uses a sin-profile. Transition form a sin-to a cos-profile is accomplished by multiplication of the complex amplitudes of the space harmonics by a phase factor exp $(-im\pi/2)$. This adjustment has been made in Tables 7a through 8d for the WS values. In the TE- case however, a discrepancy by 180^o remains which can probably be traced to a sign error.

[15] For a summary of the PO approximation method see Appendix B of Part I.

85°, geometrical shadowing occurs and PO values are given for both options, that shadowing is considered and that it is neglected. Only power densities exceeding 10^{-3} (referred to the incident power density) are shown in the tables; zeros indicate smaller magnitudes. Due to the large d/λ ratio the number of propagating space harmonics is rather large (20). At the bottom of the tables, the accumulated power of all space harmonics and the magnitude of the relative power error

$$|\epsilon| = \left| \sum_m P_m - 1 \right| \cdot 100\%$$

are given.

The tables show that for directions of incidence sufficiently far above grazing the PO method provides a good approximation of the power densities of the space harmonics, though the accuracy declines with increasing θ. At $\theta = 45^{\circ}$ and 75°, errors of 10% or more occur even for space harmonics of significant magnitude. Near grazing incidence, at $\theta = 85^{\circ}$, the PO approximation with shadowing leads to substantial errors, but may still be used to estimate the order of magnitude of the space harmonics. The PO approximation without shadowing is practically useless in this range; the power criterion is violated with an error exceeding 100%. The apparent reason for this failure is that, at incidence angles near grazing, coupling between surface cells becomes significant, in particular at TM-polarization where even a slight surface corrugation has the effect of inverting the (amplitude) reflection coefficient of a perfectly plane metal surface from +1 into -1. In contrast, the PO approach is based on the assumption that the current distribution is determined solely by local effects. In general, it appears that taking shadow effects into account improves the approximation at large d/λ. Note that for all incidence angles considered here the deviation of the total scatter power from unity (power criterion) is smaller than the power errors of individual space harmonics. Apparently these errors compensate to a certain degree in the accumulation process.

It is assumed here that the P_m values computed on the basis of the WS theory are sufficiently accurate to serve as a standard for judging the accuracy of the PO approximation. As justificaiton we point to the very high accuracy with which the WS values satisfy the power criterion at all θ values considered. For a further discussion of the limitations of the PO approximation we refer to Zaki and Neureuther [6]

Observe that at large angles of incidence the magnitude of the specular reflected wave (spectral order $m = 0$) is very small for TM-polarization, but dominant for TE-polarization [16]. This is in agreement with the trend, noted for surfaces of moderate groove width, that in the range of large incidence angles TM-polarization leads to substantially less specular reflection and a more even distribution of the incident power over the spectrum of space harmonics than TE-polarization.

---

[16] For $\theta = 90^{\circ}$, the power of the specular reflected wave, of course, approaches unity for either polarization.

6. ACKNOWLEDGEMENTS

The authors wish to thank Mrs. H. Perlman for writing the computer program and Mr. L. Leskowitz of the ECOM Math. Analysis Section for assistance in adapting existing programs to computers at ECOM. Thanks are extended to Messrs. P. Demko and R. Boriss of Avionics Laboratory for their continued interest in this study. Thanks are due Drs. G. Goubau and J. Mink for helpful discussions. The authors are grateful to Dr. Zaki of the University of Maryland and Dr. Neureuther of the University of California for making their program available and providing instructions for its use.

This study was conducted jointly by the Communications/Automatic Data Processing Laboratory, ECOM, and the New Jersey Institute of Technology during the summers of 1973 and 1974. During these periods, Dr. G. Whitman, the co-author of this report, worked with the Antenna Team of the Communications/Automatic Data Processing Lab., under the Laboratory Research Cooperative Program.

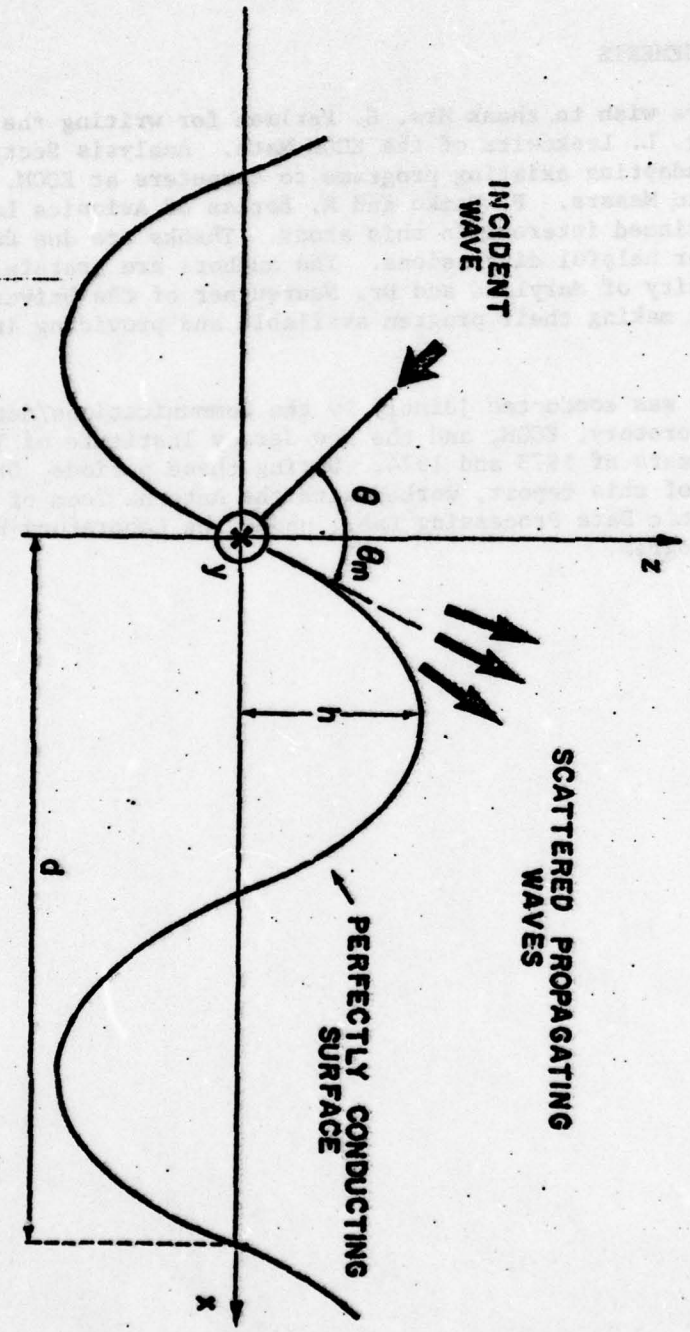

Fig. 1. Sinusoidal metal surface illuminated by plane wave. Coordinates and geometrical parameters used in analysis of scatter problem.

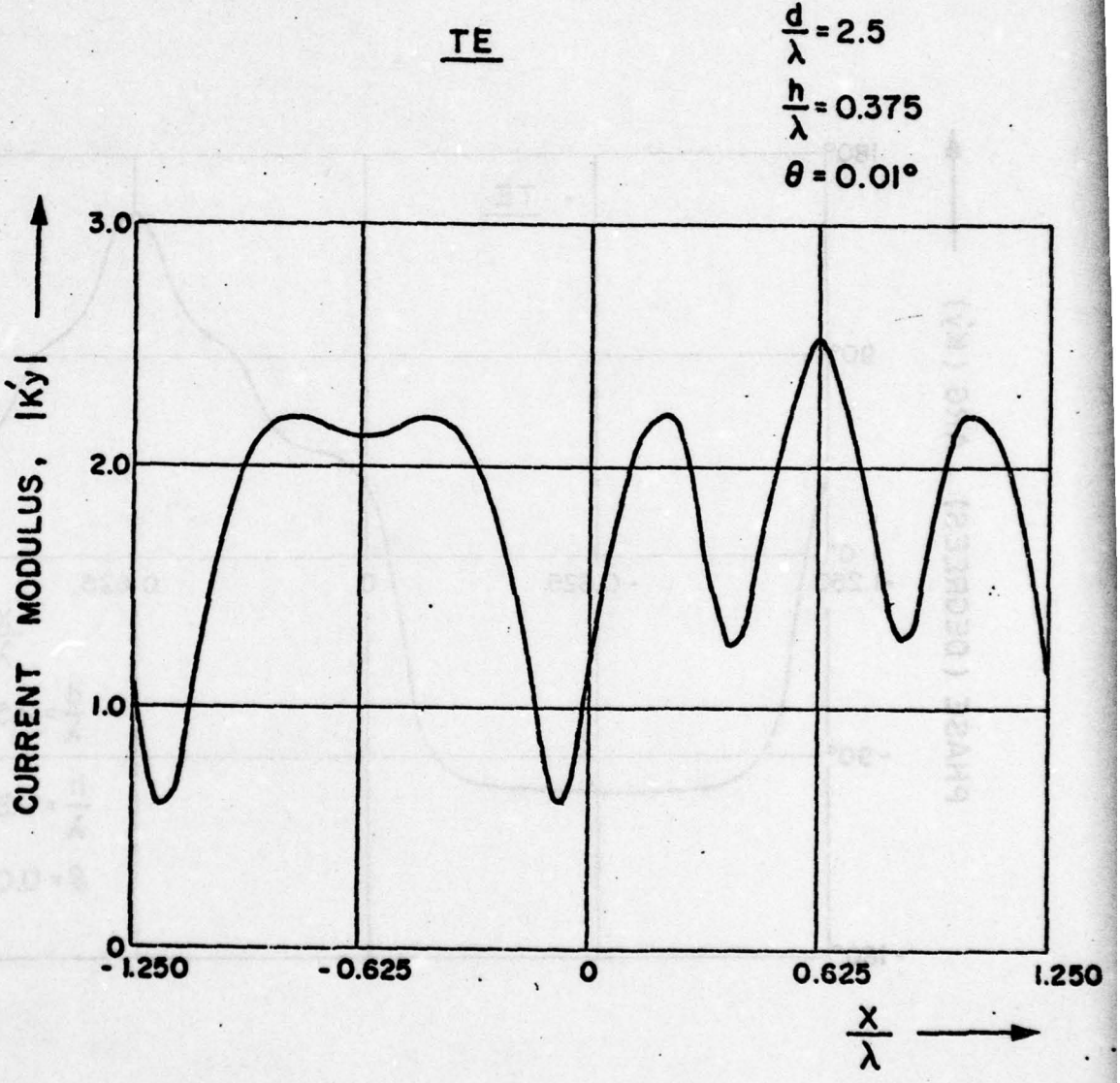

Fig. 2a Modulus of current distribution over one period of sinusoidal metal surface illuminated by TE-polarized plane wave incident at $\theta = 0.01^{\circ}$.

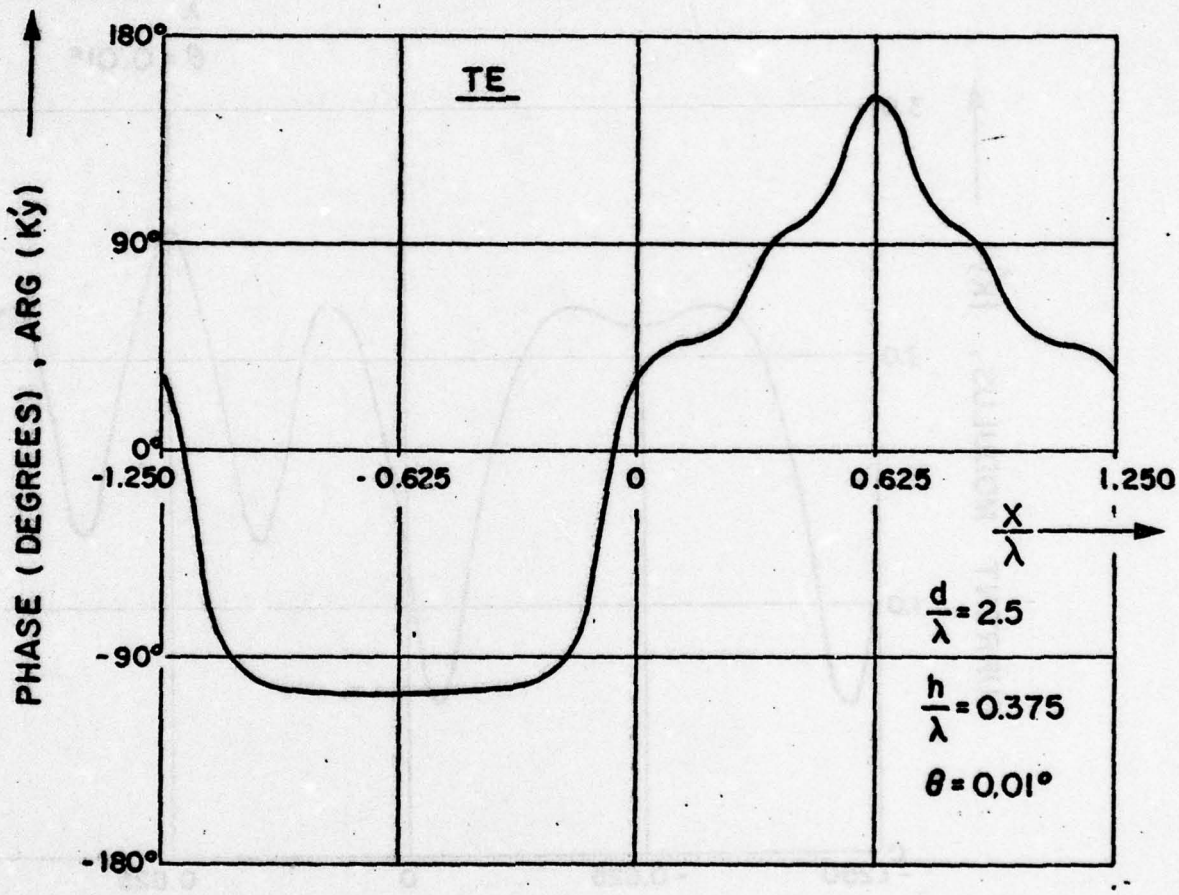

Fig. 2b. Phase of current distribution over one period of sinusoidal metal surface illuminated by TE-polarized plane wave incident at $\theta = 0.01^{\circ}$.

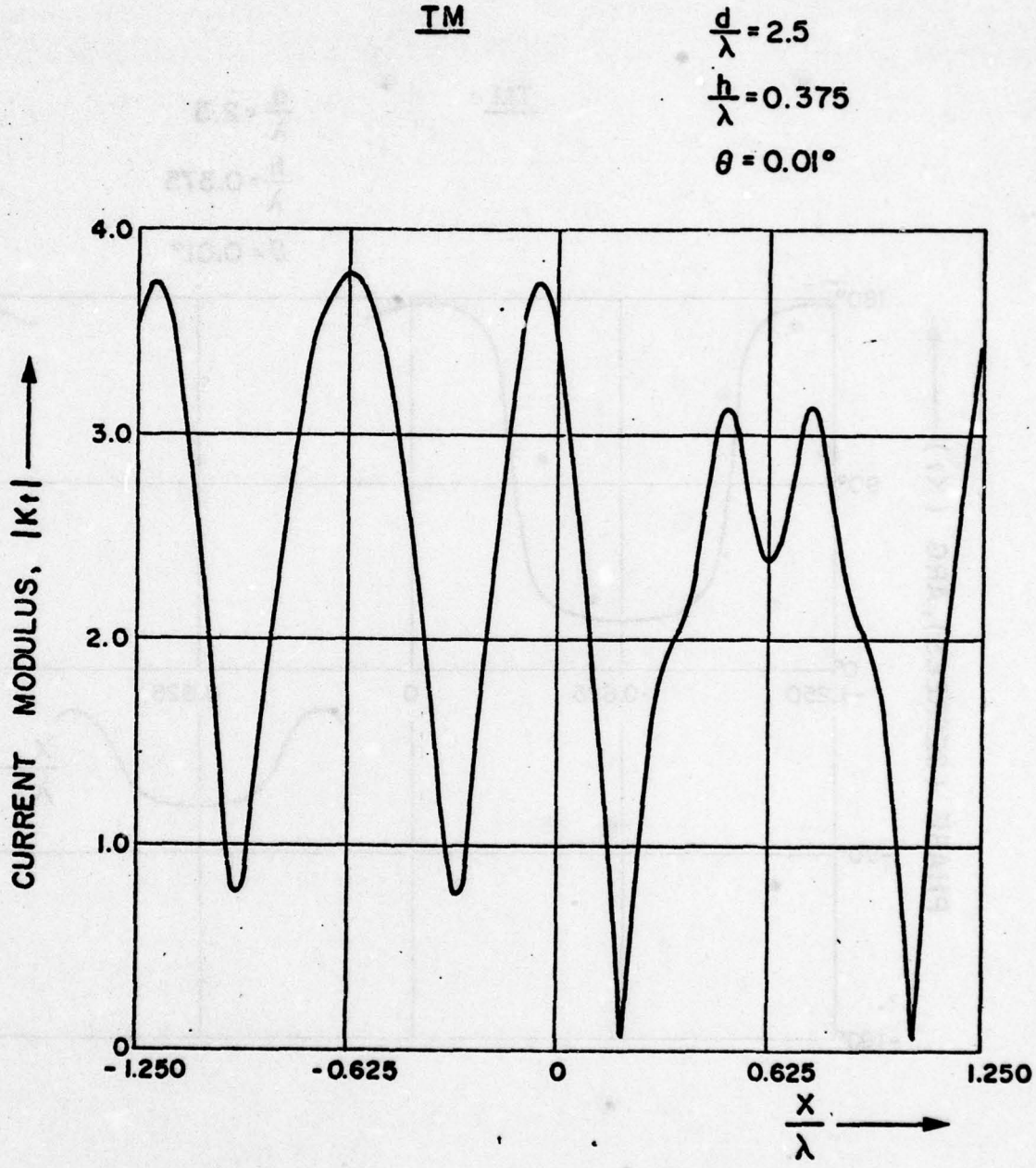

Fig. 3a. Modulus of current distribution over one period of sinusoidal metal surface illuminated by TM-polarized plane wave incident at $\theta = 0.1^{\circ}$.

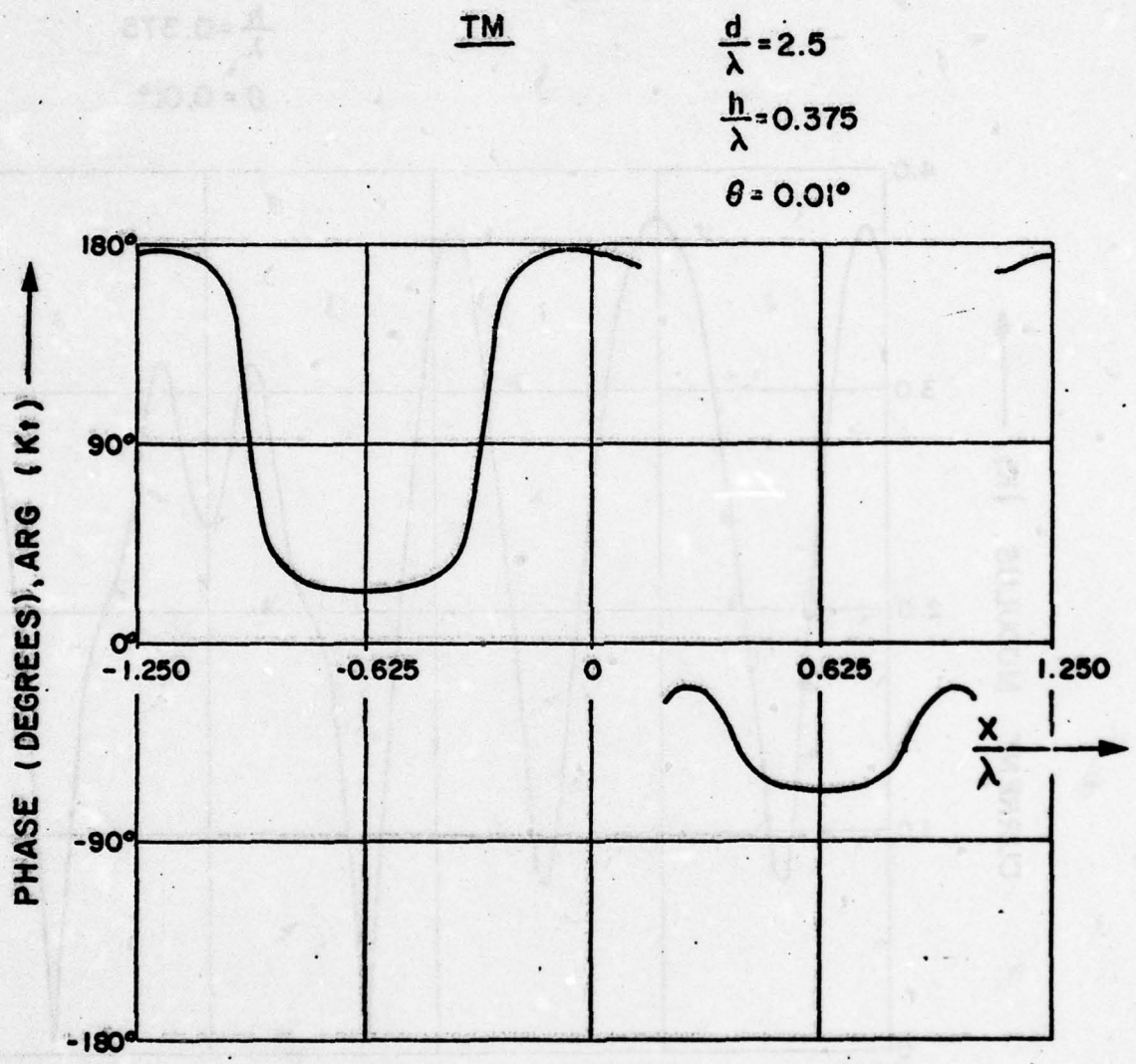

Fig. 3b. Phase of current distribution over one period of sinusoidal metal surface illuminated by TM-polarized plane wave incident at $\theta = 0.01^{\circ}$.

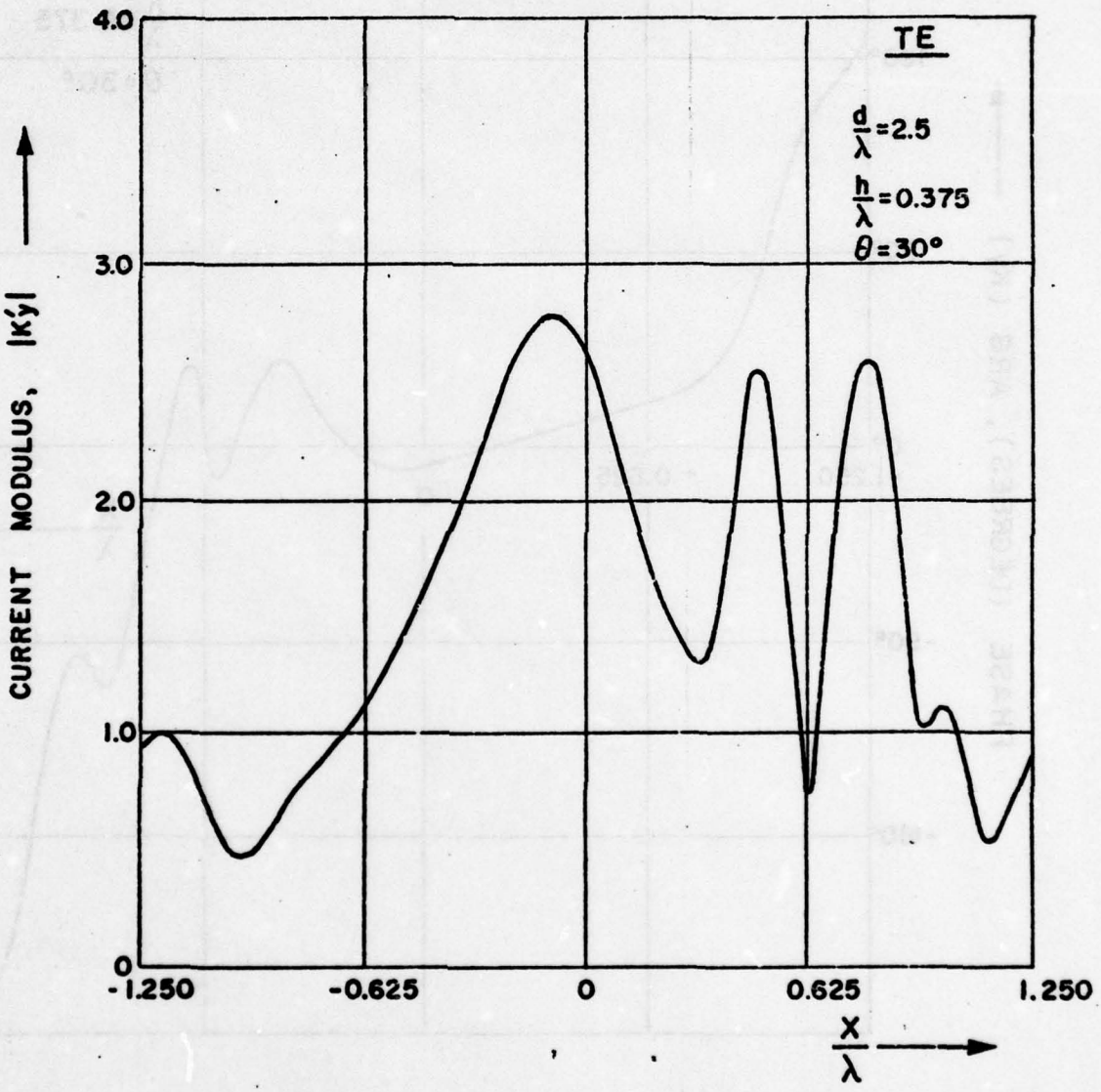

Fig. 4a. Modulus of current distribution over one period of sinusoidal metal surface illuminated by TE-polarized plane wave incident at $\theta = 30^{\circ}$.

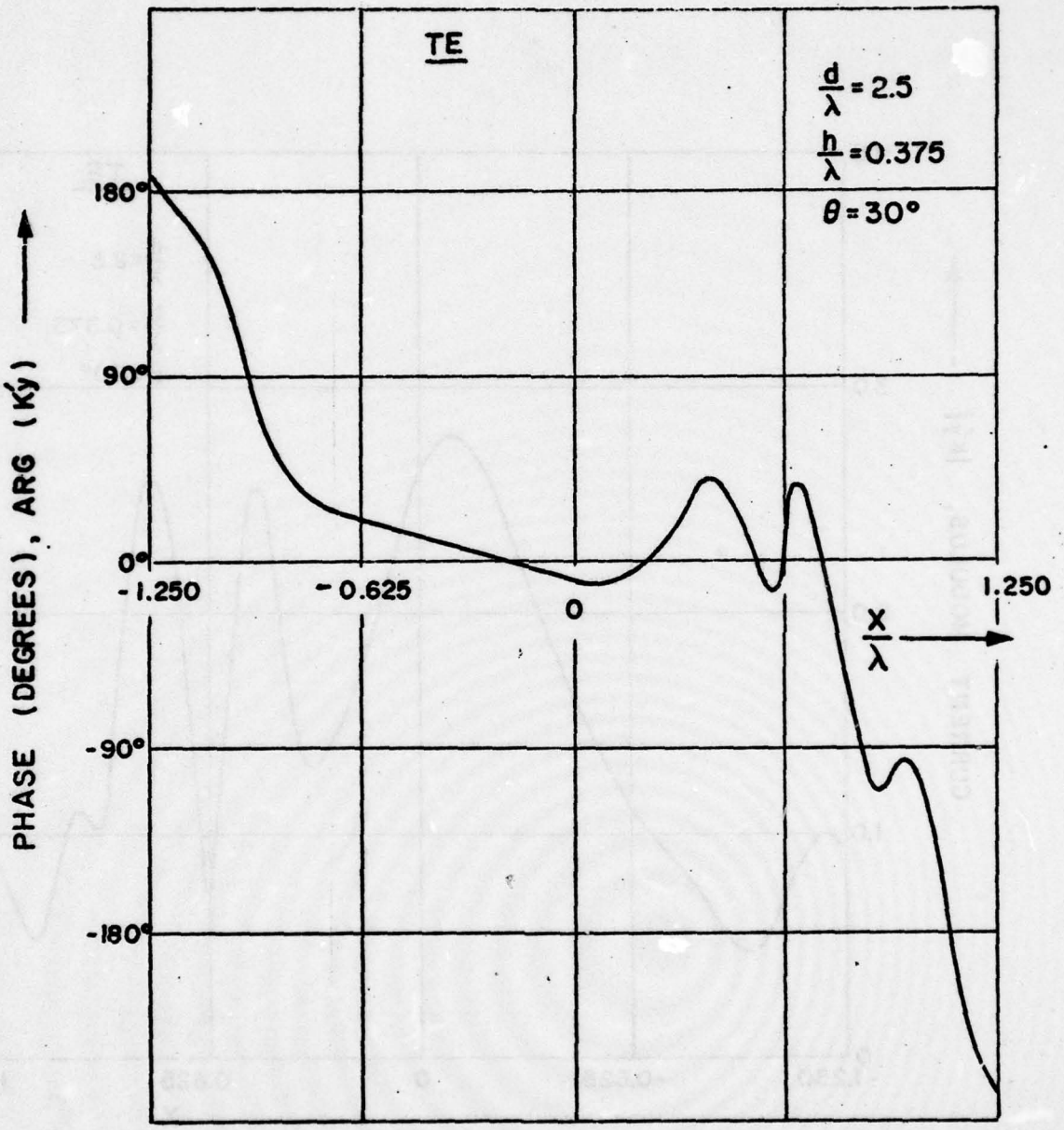

Fig. 4b. Phase of current distribution over one period of sinusoidal metal surface illuminated by TE-polarized plane wave incident at $\theta = 30^{\circ}$.

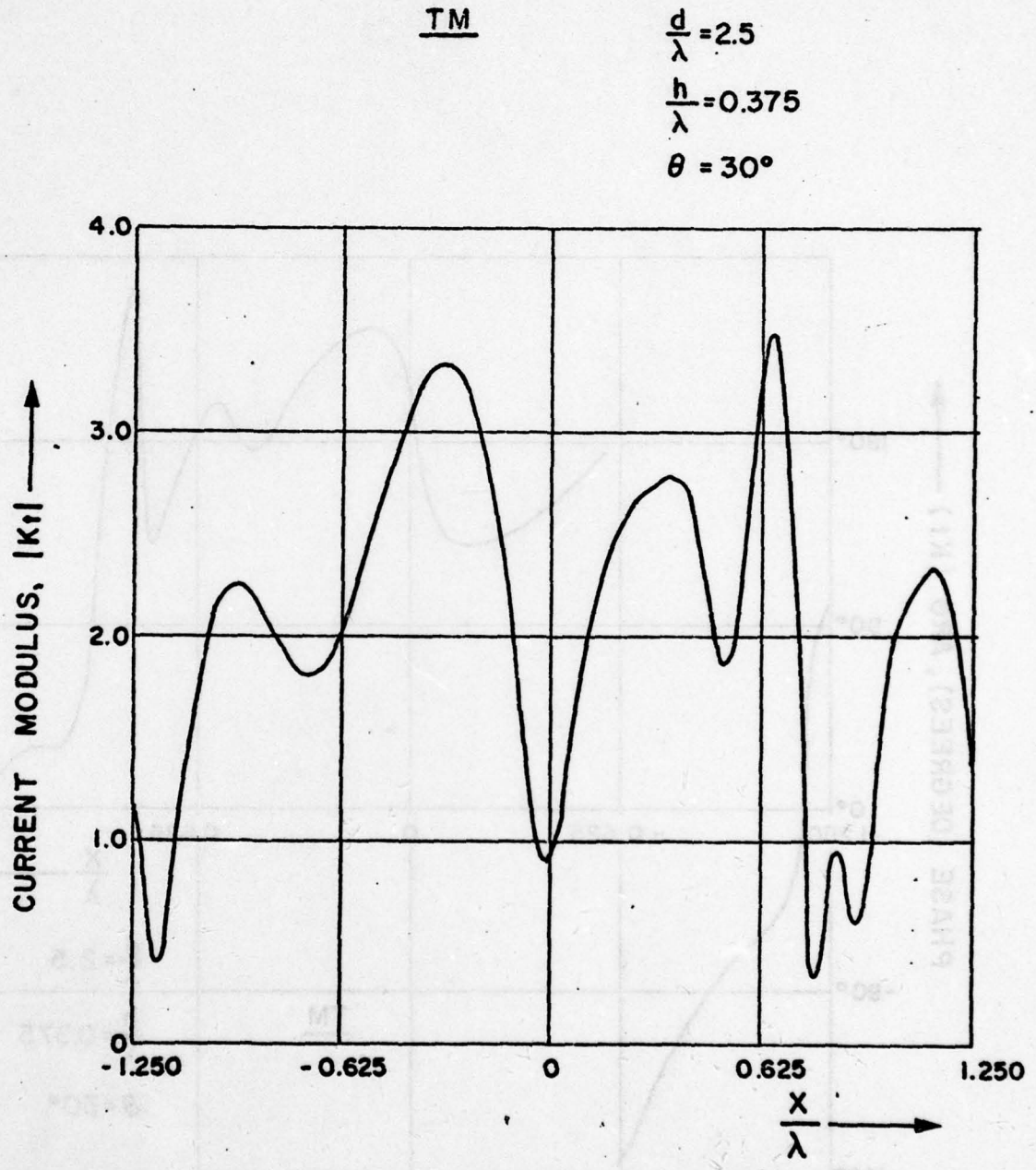

Fig. 5a. Modulus of current distribution over one period of sinusoidal metal surface illuminated by TM-polarized plane wave incident at $\theta = 30^{\circ}$.

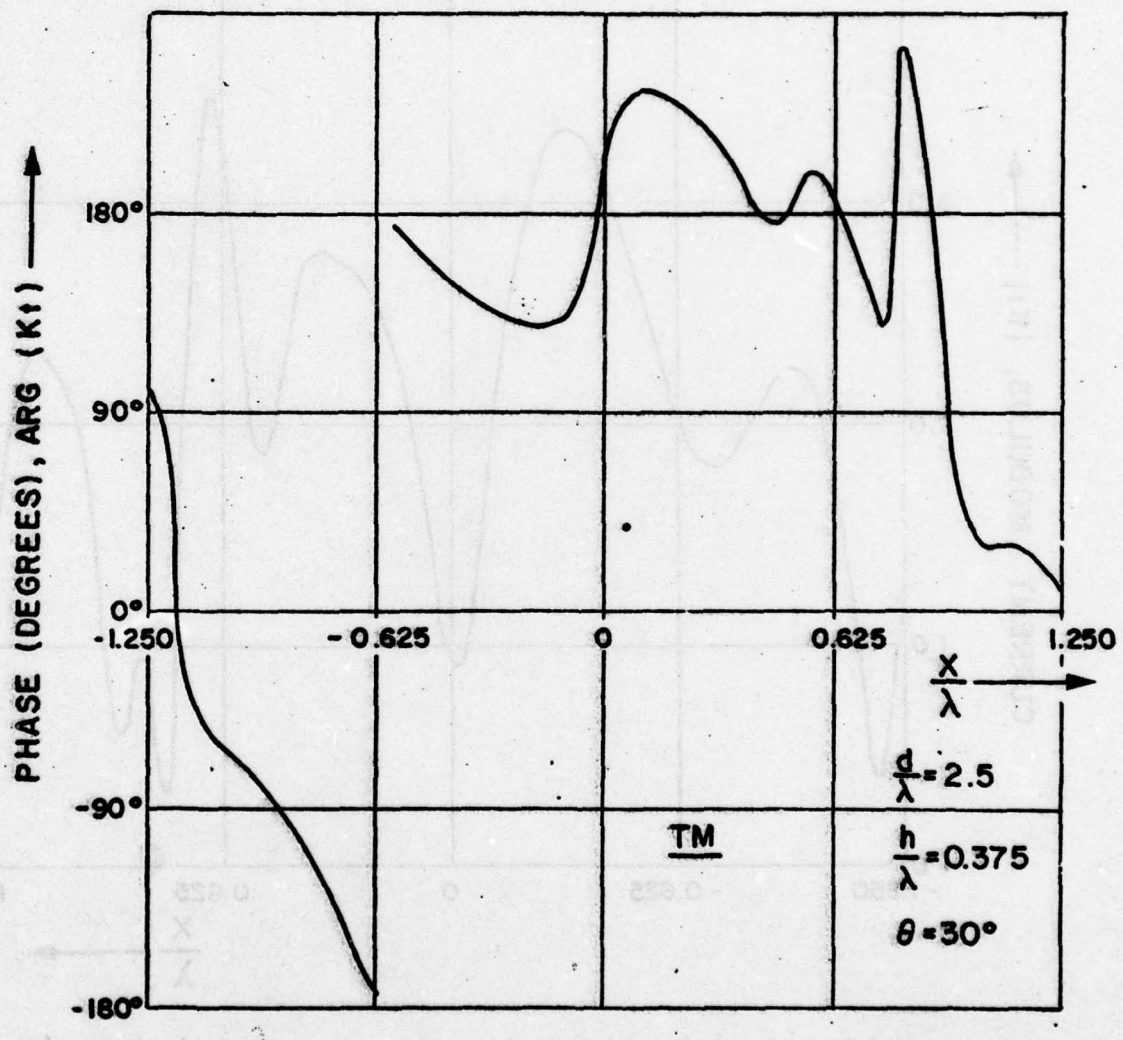

Fig. 5b. Phase of current distribution over one period of sinusoidal metal surface illuminated by TM-polarized plane wave incident at $\theta = 30^{\circ}$.

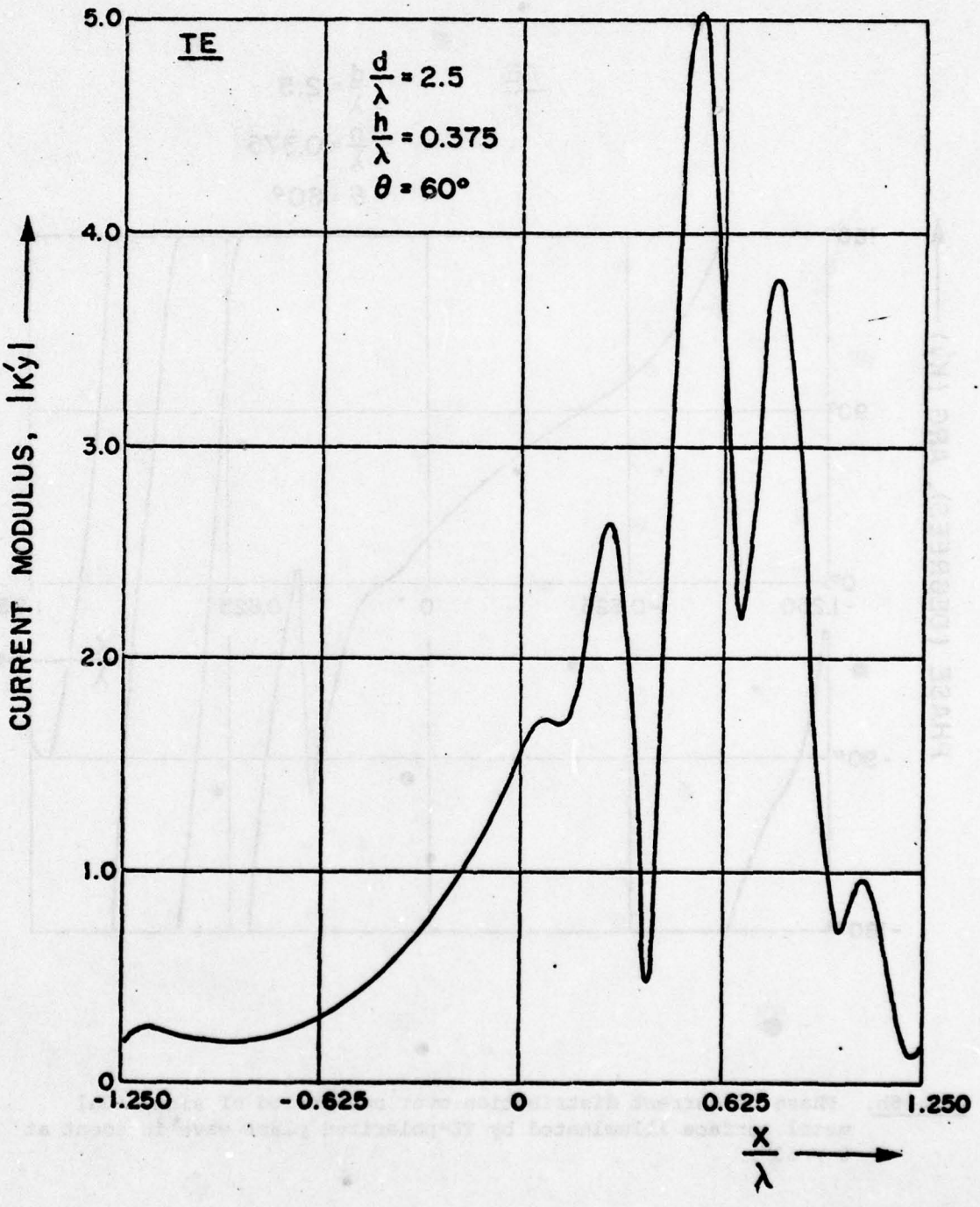

Fig. 6a. Modulus of current distribution over one period of sinusoidal metal surface illuminated by TE-polarized plane wave incident at $\theta = 60^{\circ}$.

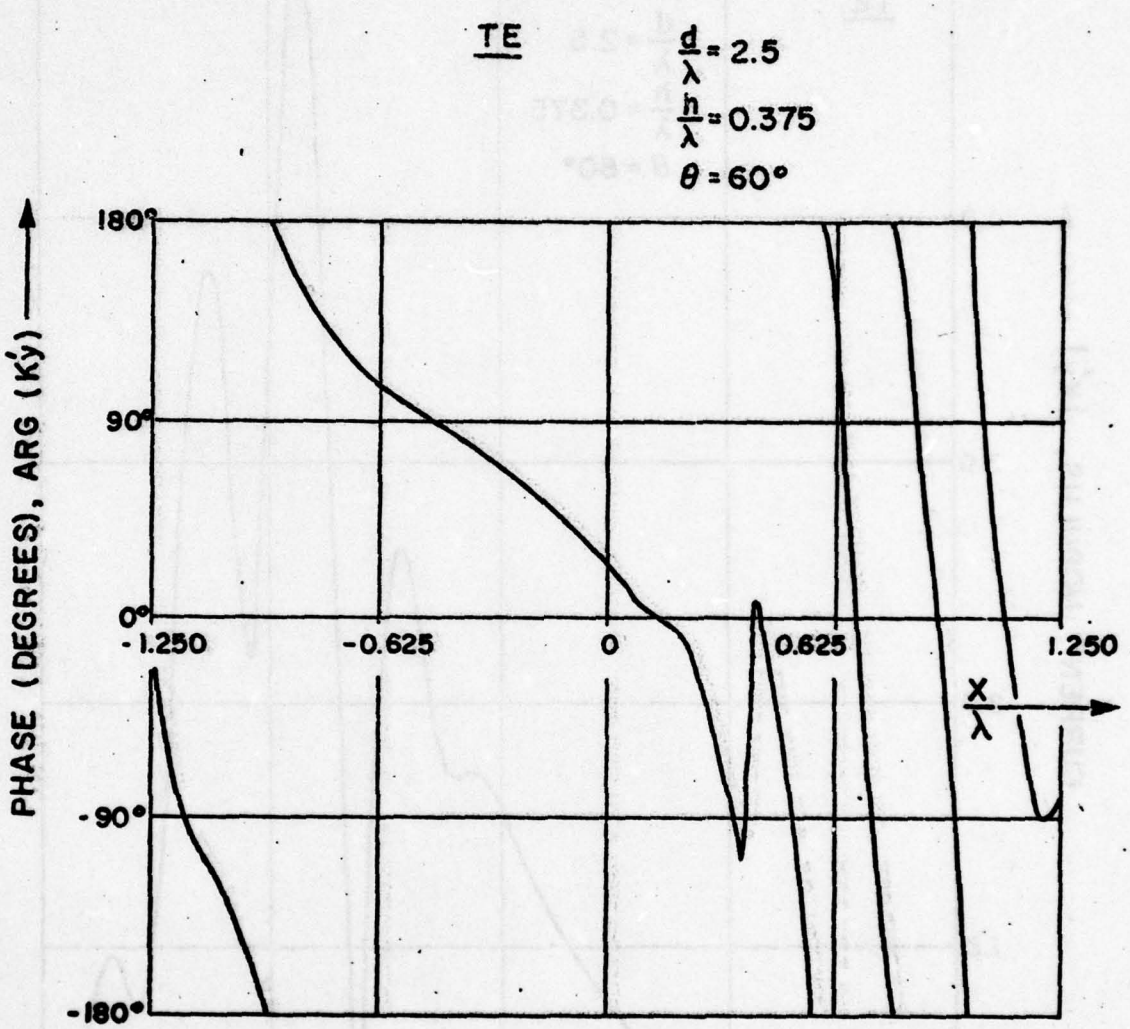

Fig. 6b. Phase of current distribution over one period of sinusoidal metal surface illuminated by TE-polarized plane wave incident at $\theta = 60^{\circ}$.

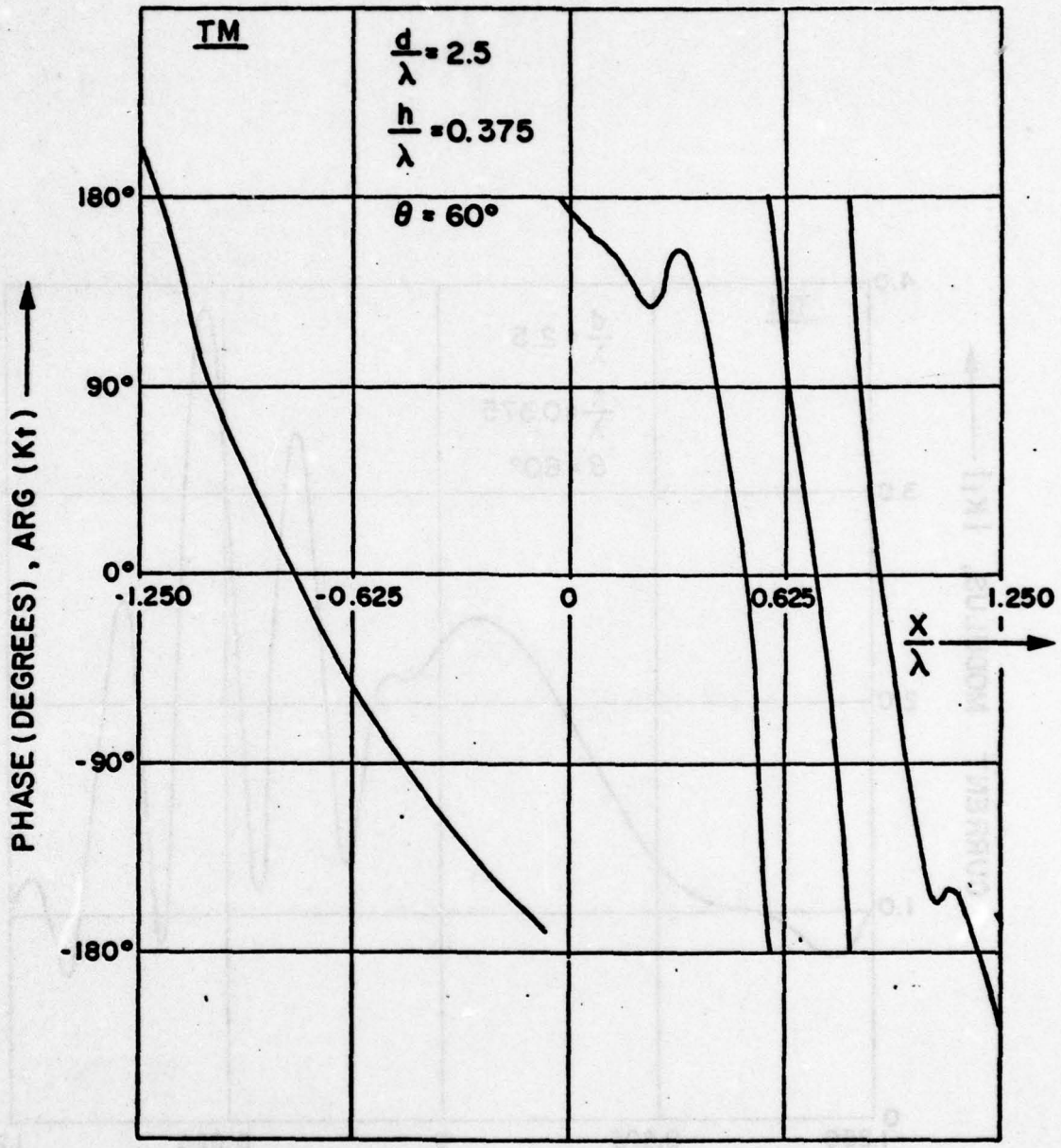

Fig. 7a. Modulus of current distribution over one period of sinusoidal metal surface illuminated by TM-polarized plane wave incident at $\theta = 60^{\circ}$.

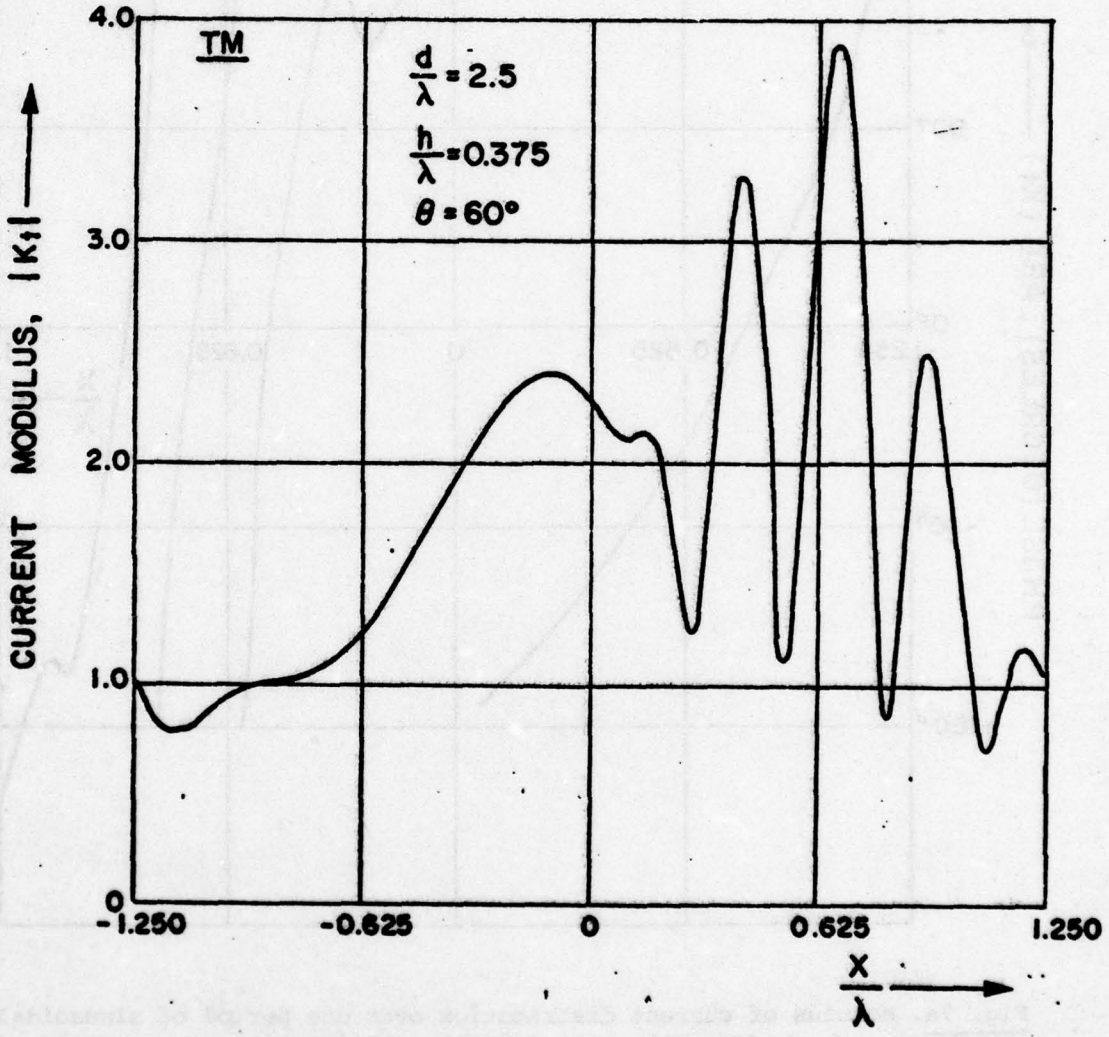

Fig. 7b. Phase of current distribution over one period of sinusoidal metal surface illuminated by TM-polarized plane wave incident at θ = 60°.

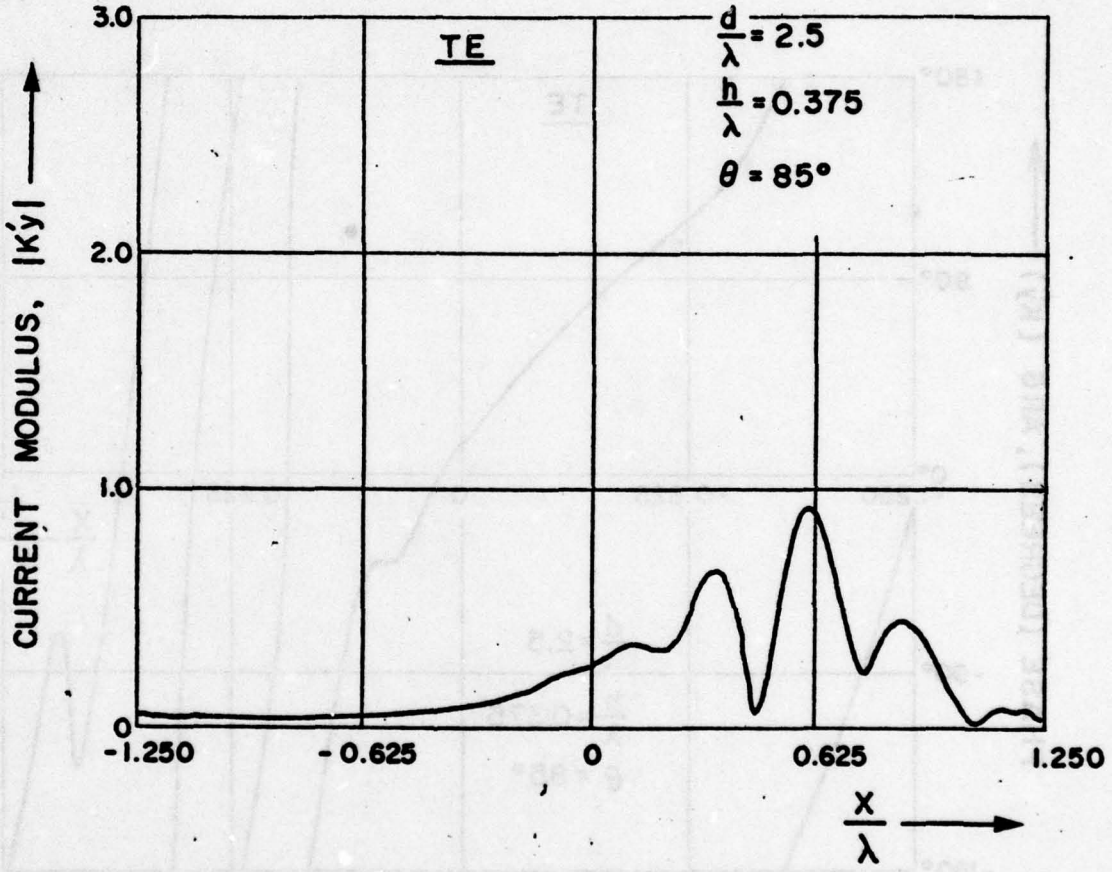

Fig. 8a. Modulus of current distribution over one period of sinusoidal metal surface illuminated by TE-polarized plane wave incident at $\theta = 85^{\circ}$.

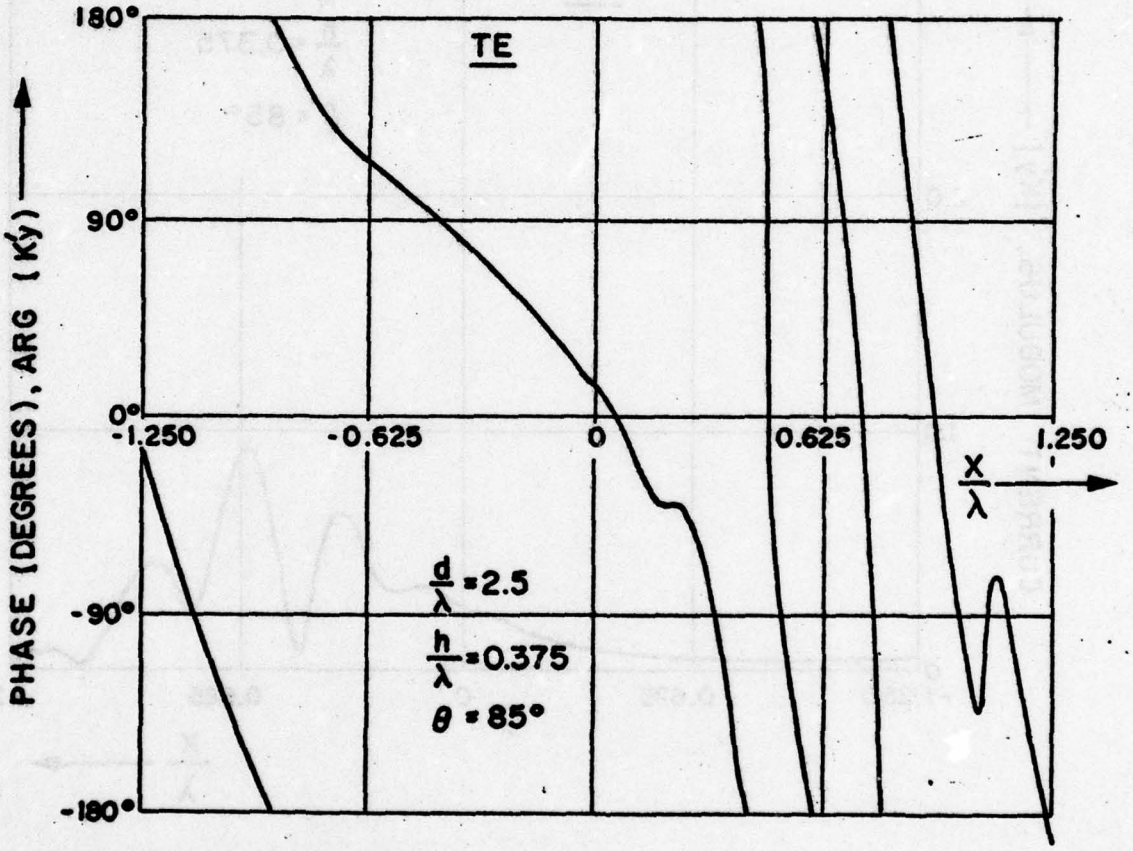

Fig. 8b. Phase of current distribution over one period of sinusoidal metal surface illuminated by TE-polarized plane wave incident at $\theta = 85^{\circ}$.

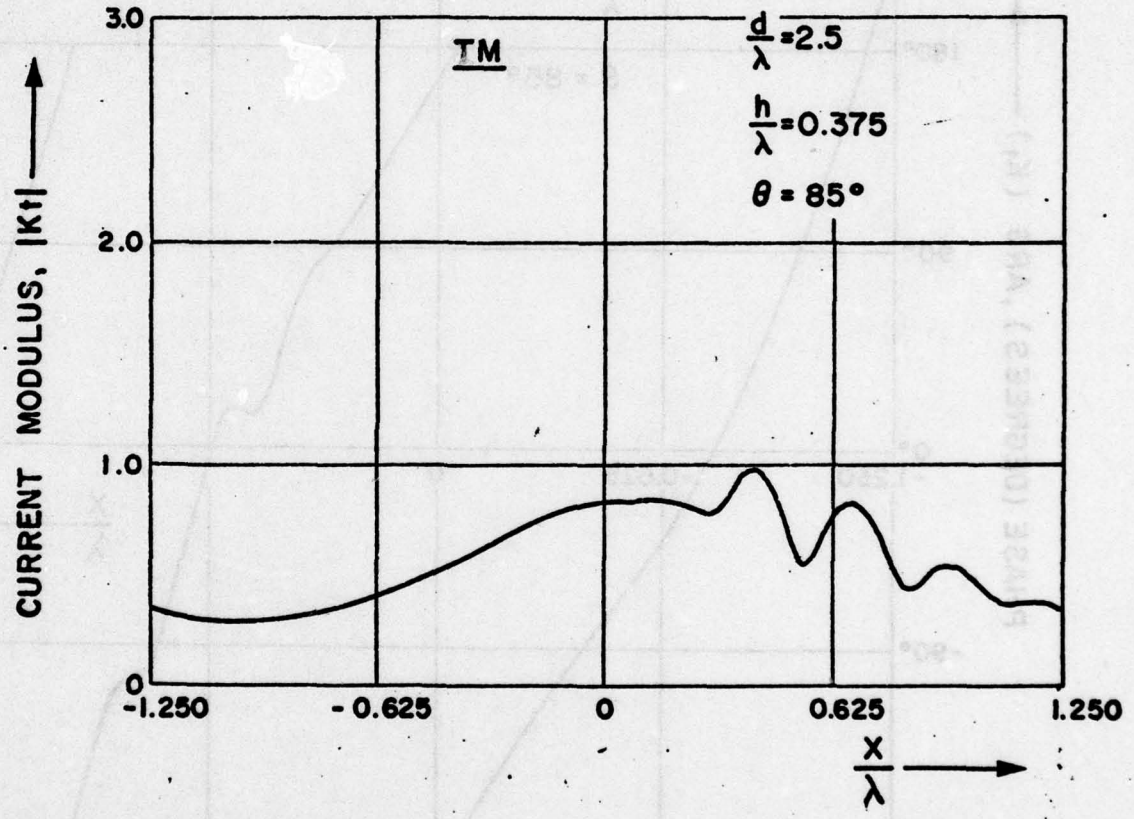

Fig. 9a. Modulus of current distribution over one period of sinusoidal metal surface illuminated by TM-polarized plane wave incident at $\theta = 85^{\circ}$.

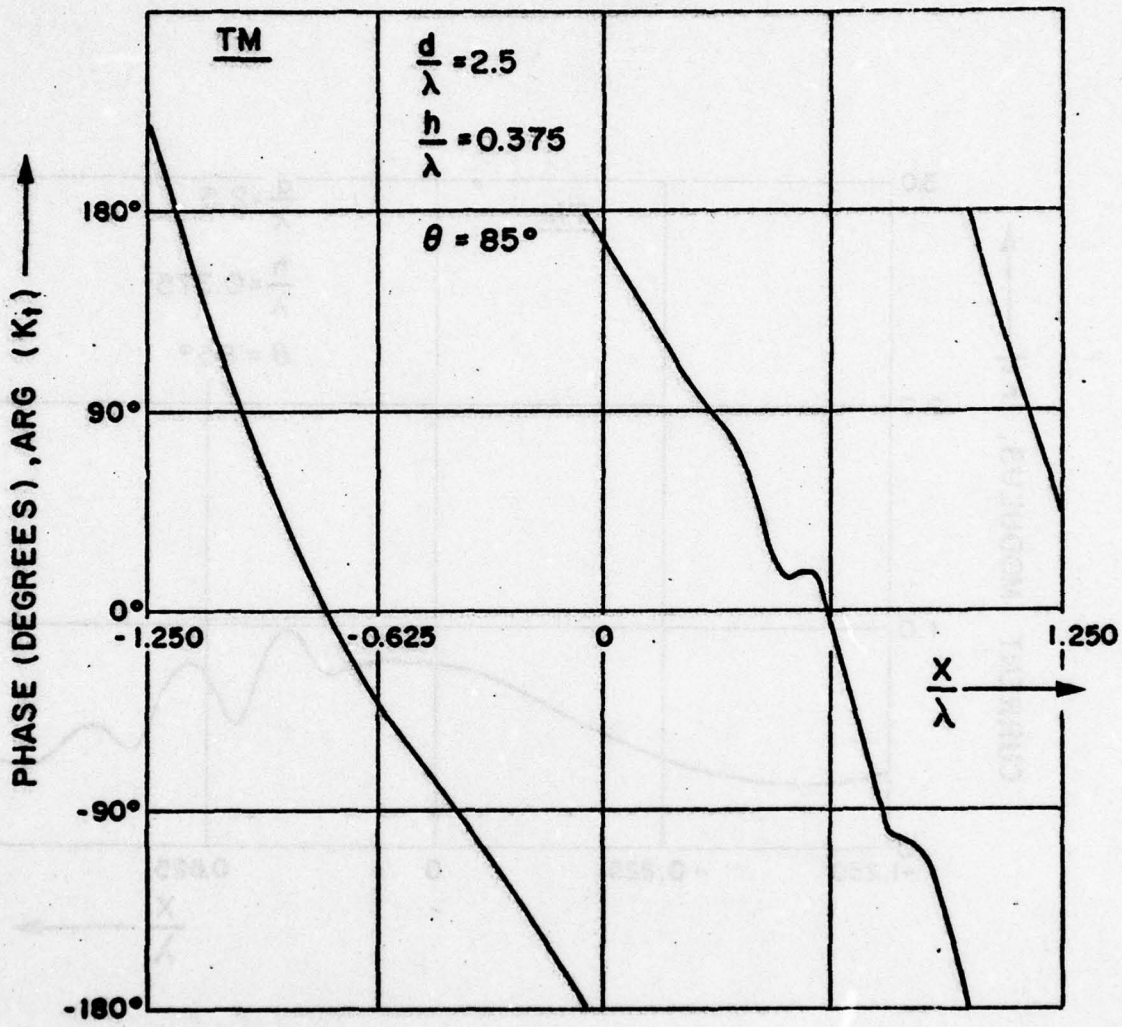

Fig. 9b. Phase of current distribution over one period of sinusoidal metal surface illuminated by TM-polarized plane wave incident at $\theta = 85^{\circ}$.

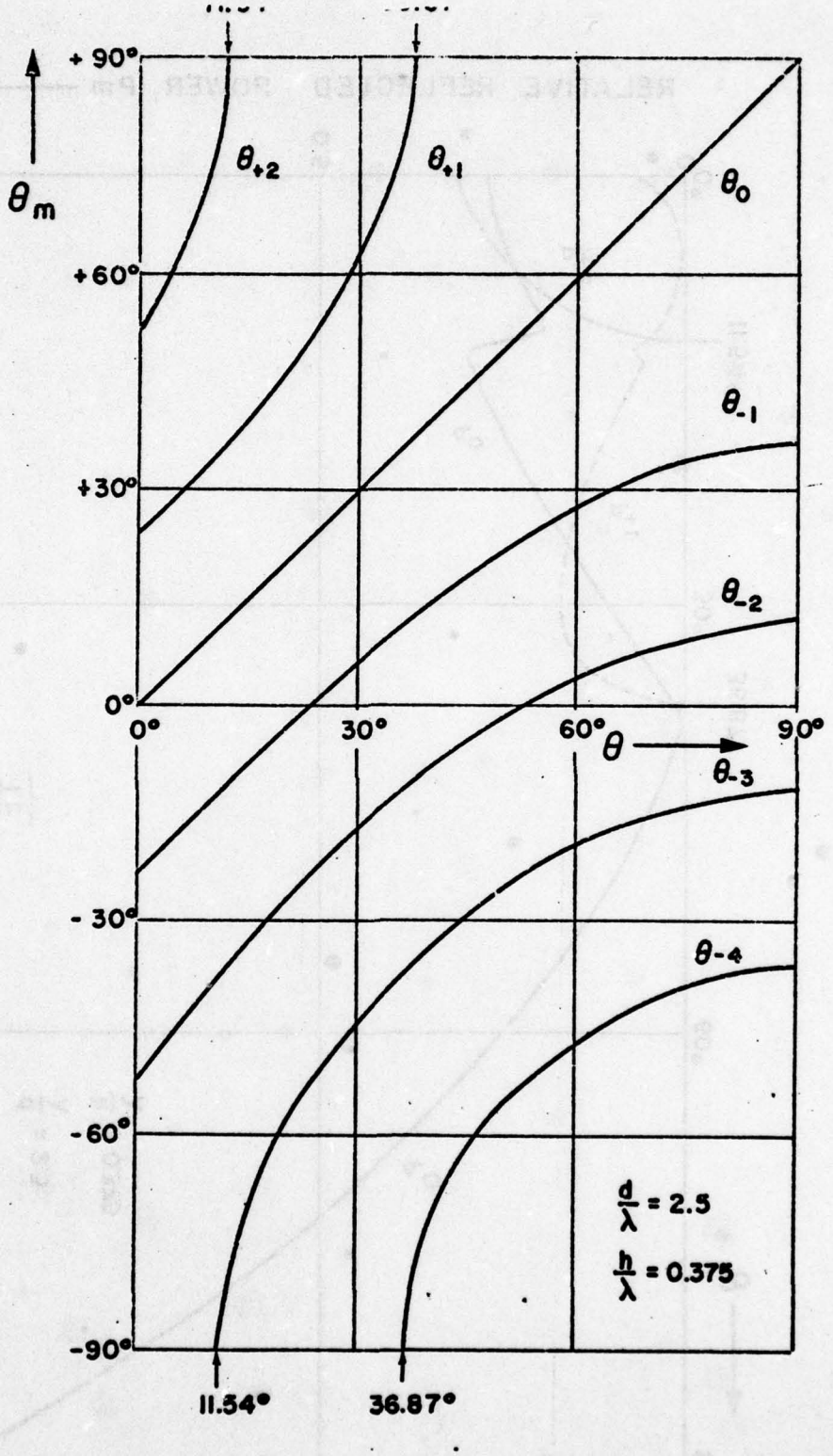

Fig. 10. Direction angles θ_m of propagating space harmonics of scatter field vs. incidence angle θ of primary plane wave ($d/\lambda = 2.5$).

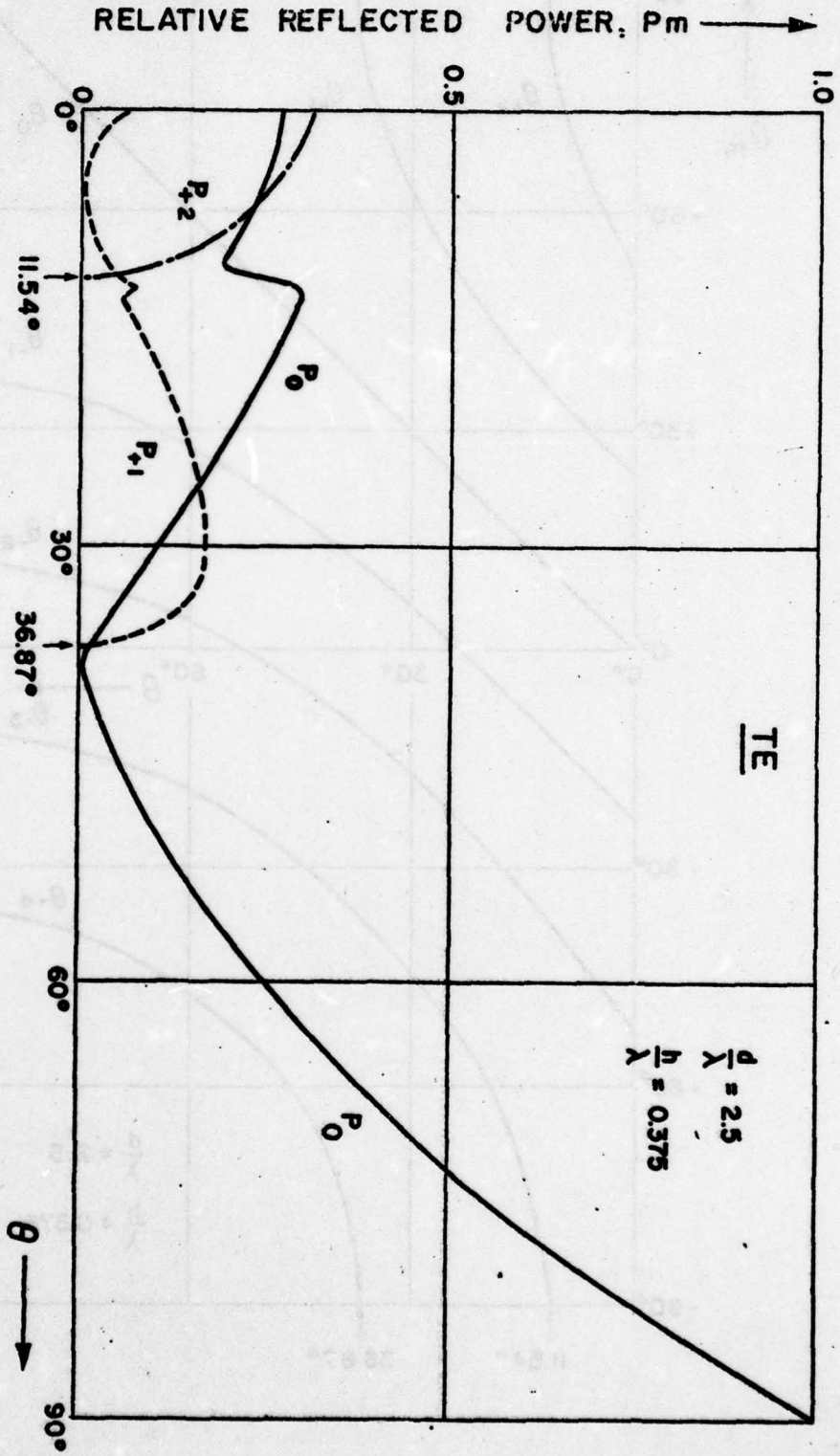

Fig. 11a. Powers P_m of propagating space harmonics vs. incident angle θ of primary wave. Spectral orders: m = +2,+1,0. Polarization: TE. Surface parameters: $d/\lambda = 2.5$, $h/\lambda = 0.375$.

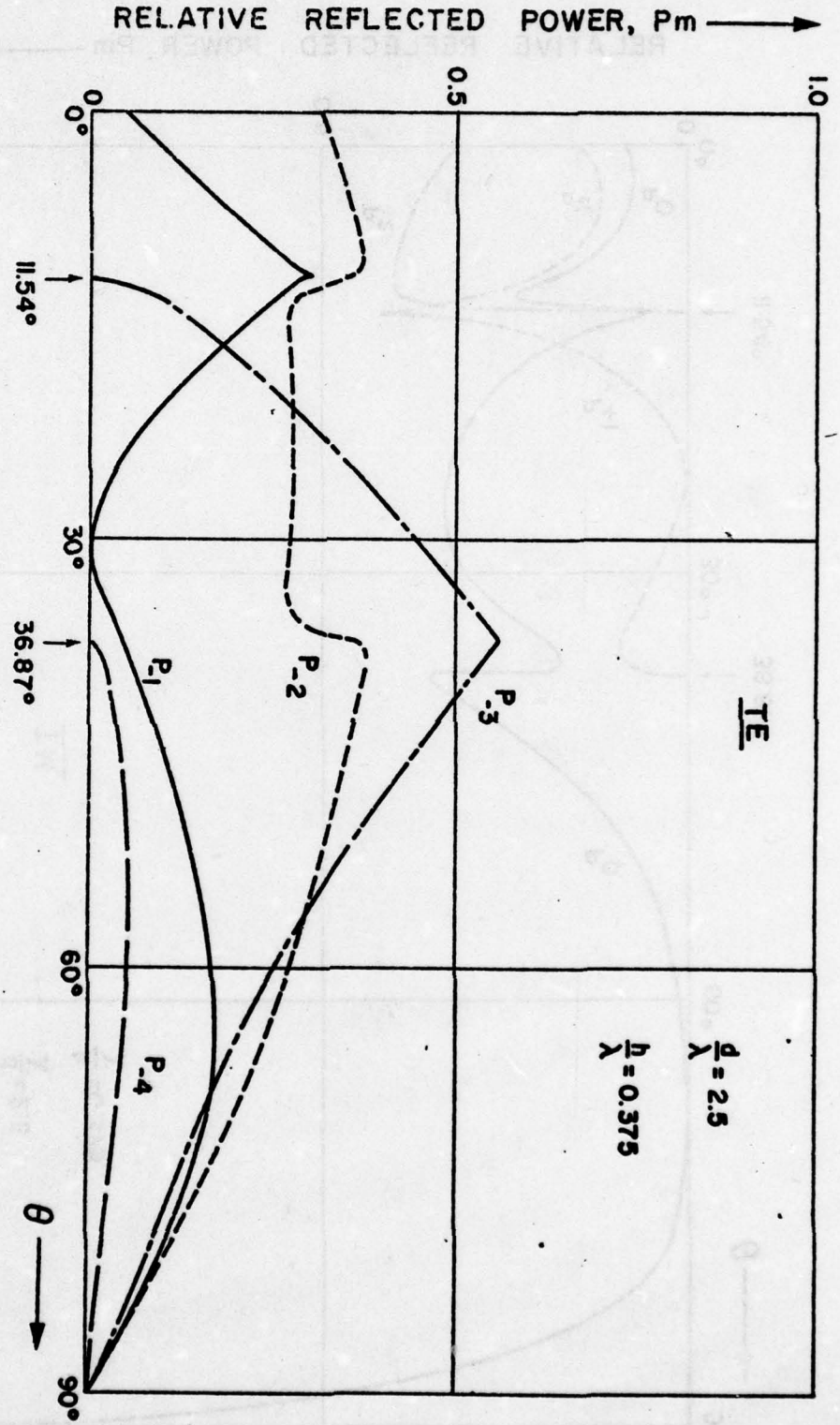

Fig. 11b. Powers P_m of propagating space harmonics vs. incident angle θ of primary wave. Spectral orders: m = -1, -2, -3, -4. Polarization: TE. Surface parameters: $d/\lambda = 2.5$, $h/\lambda = 0.375$.

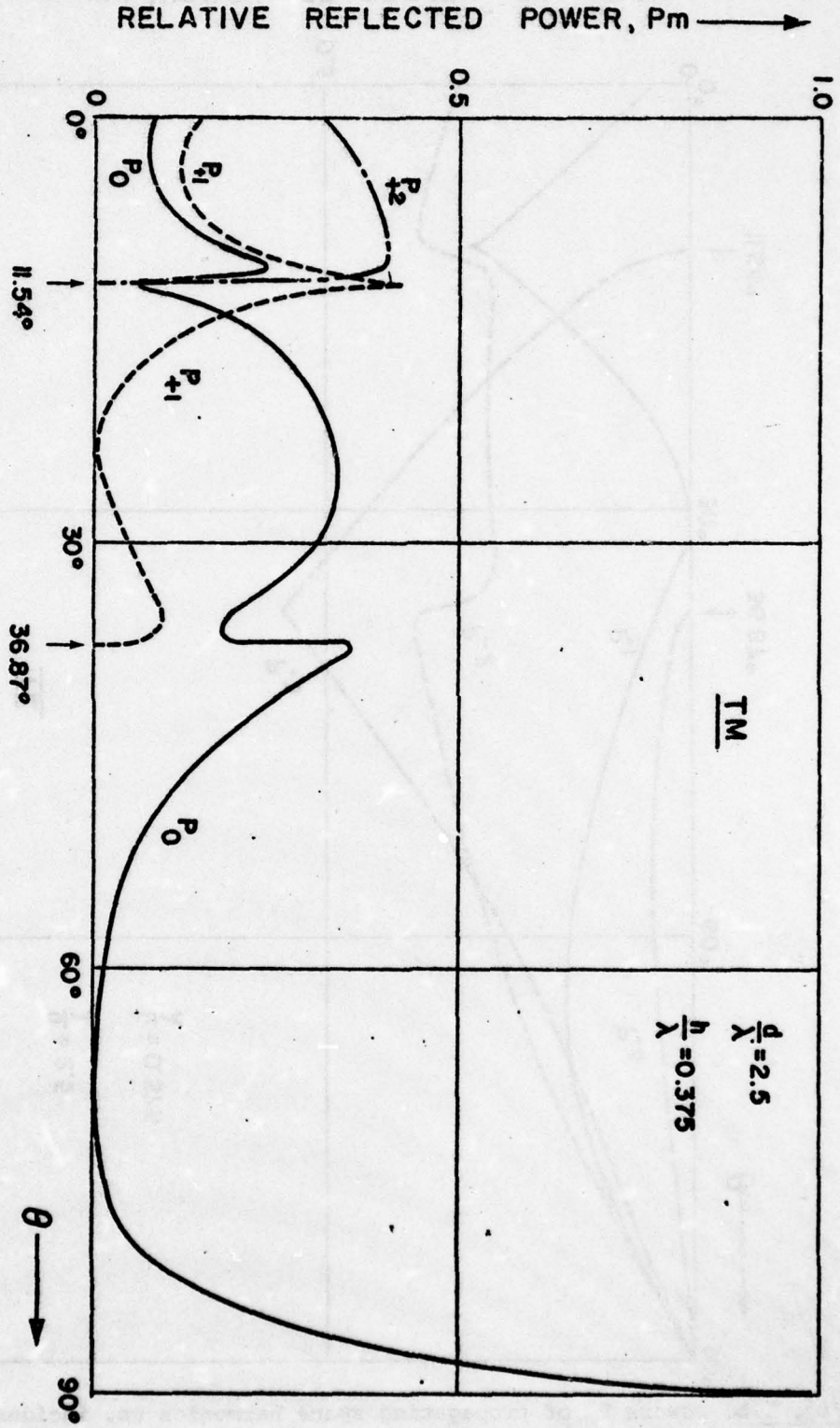

Fig. 12a. Powers P_m of propagating space harmonics vs. incidence angle θ of primary wave. Spectral orders: m = +2,+1,0. Polarization: TM. Surface parameters: $d/\lambda = 2.5$, $h/\lambda = 0.375$.

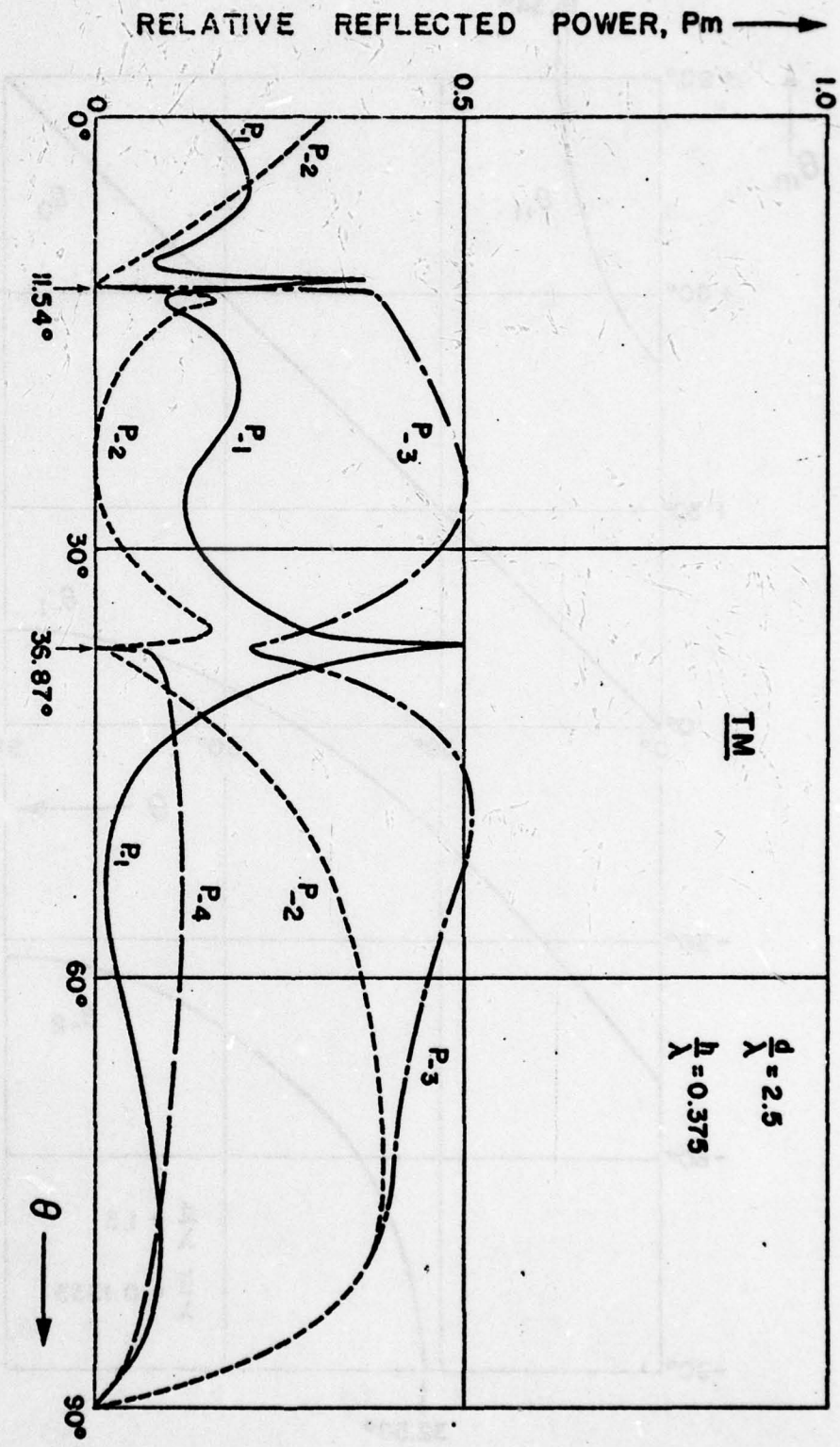

Fig. 12b. Powers P_m of propagating space harmonics vs. incidence angle θ of primary wave. Spectral orders: m = -1,-2,-3,-4. Polarization: TM. Surface parameters: $d/\lambda = 2.5$, $h/\lambda = 0.375$.

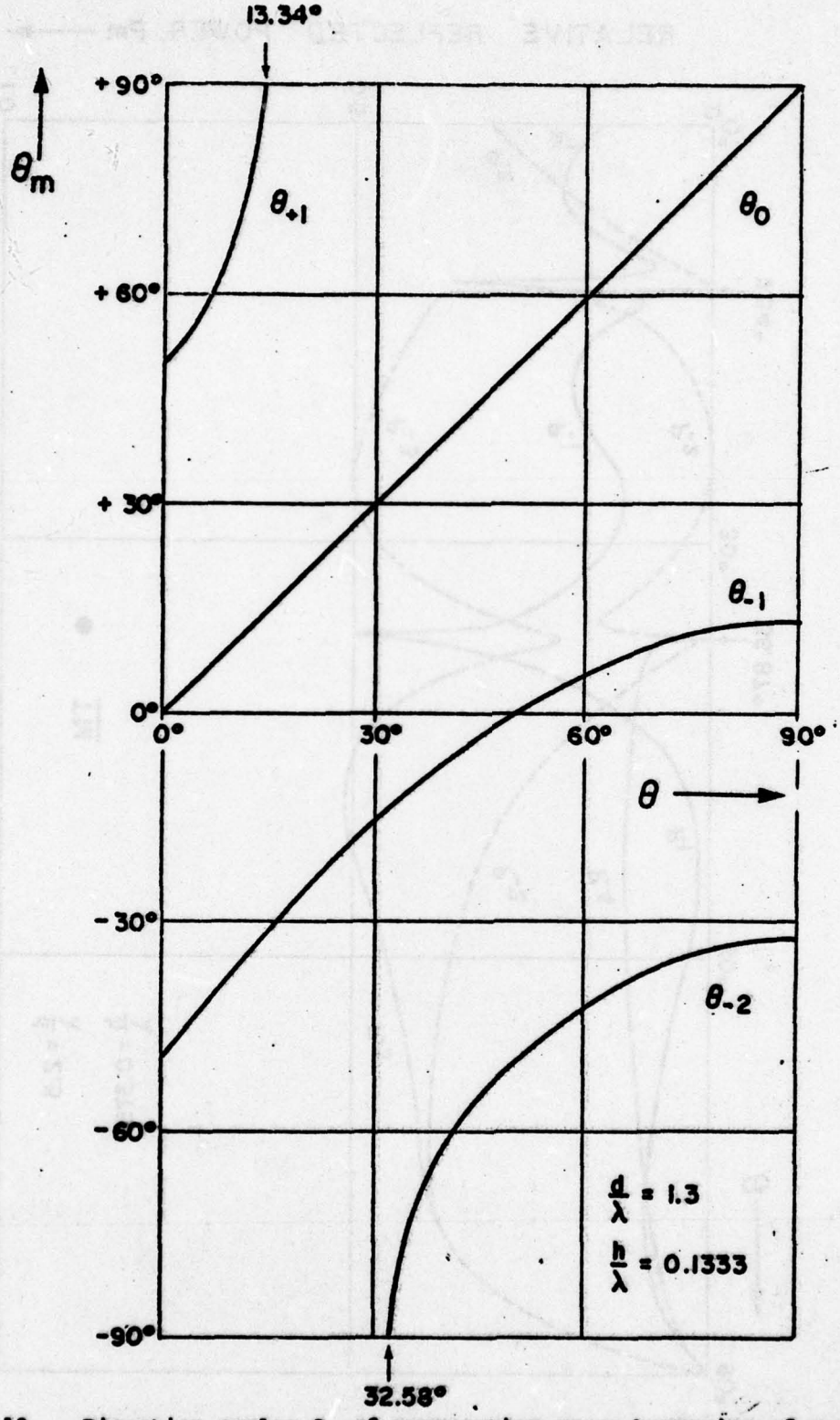

Fig.13. Direction angles θ_m of propagating space harmonics of scatter field vs. incidence angle θ of primary plane wave (d/λ = 1.3).

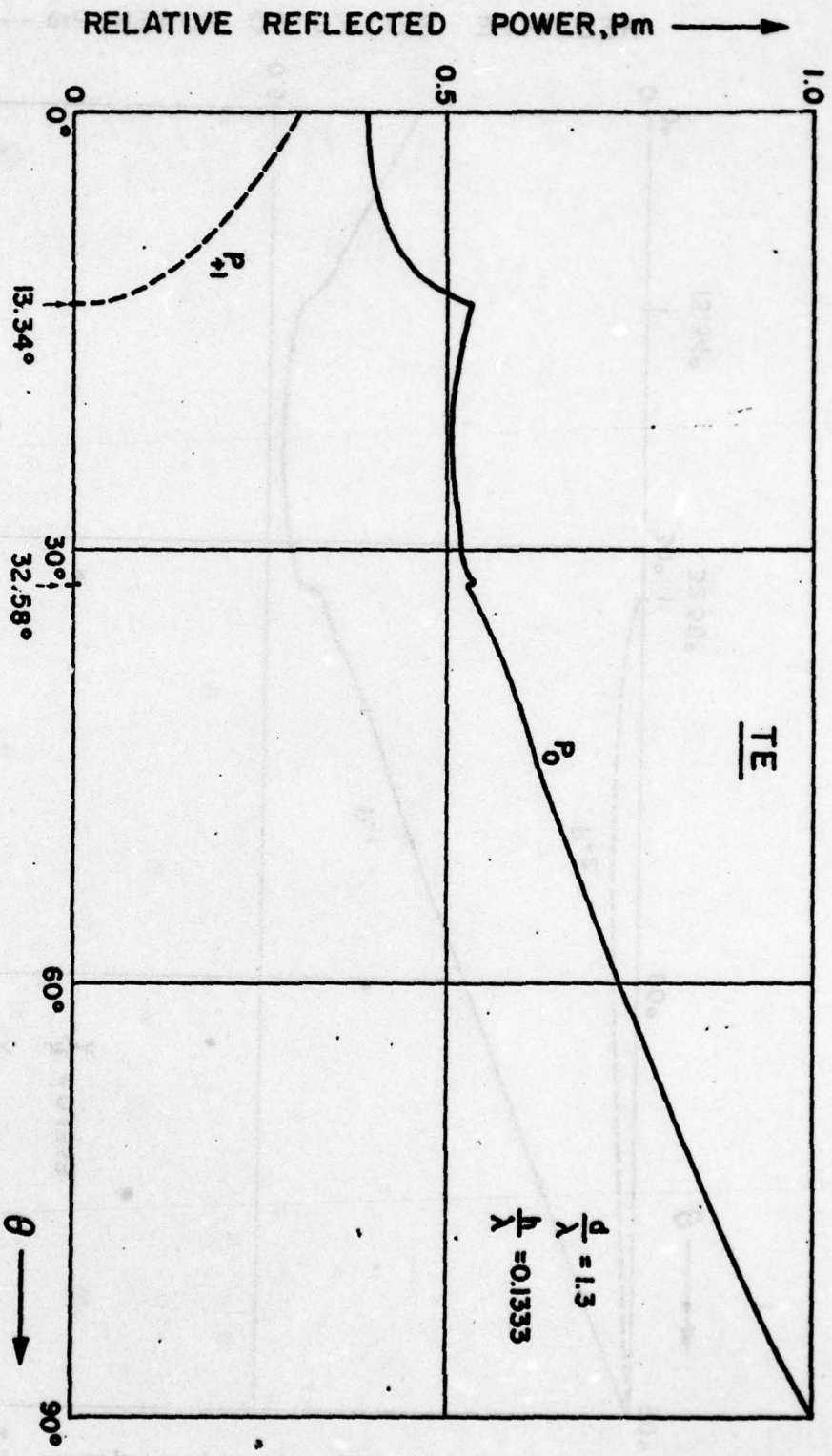

Fig. 14a. Powers P_m of propagating space harmonics vs. incidence angle θ of primary wave. Spectral orders: m = +1,0. Polarization: TE. Surface parameters: $d/\lambda = 1.3$, $h/\lambda = 0.1333$.

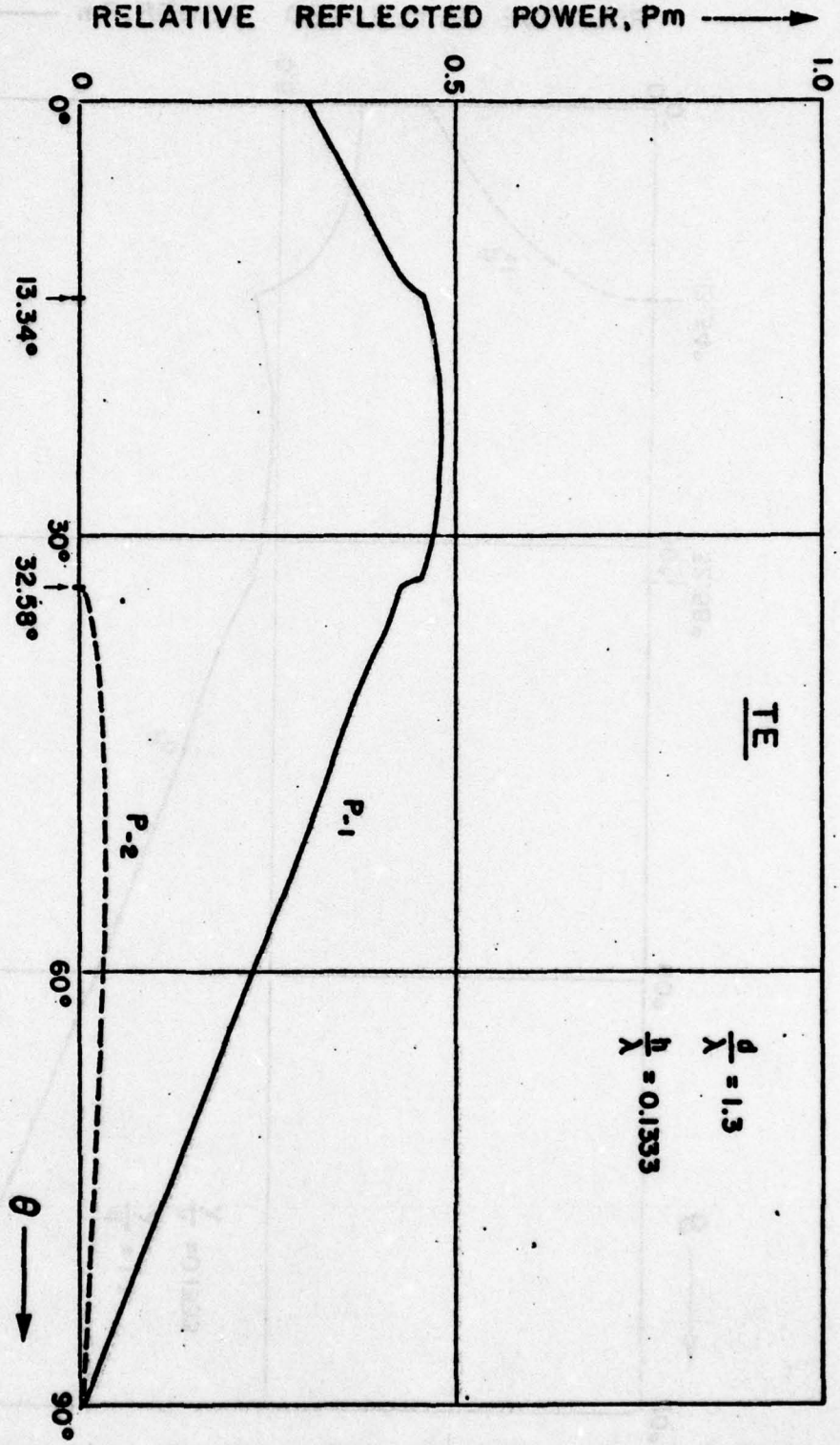

Fig. 14b. Powers P_m of propagating space harmonics vs. incidence angle θ of primary wave. Spectral orders: m = -1,-2. Polarization: TE. Surface parameters: $d/\lambda = 1.3$, $h/\lambda = 0.1333$.

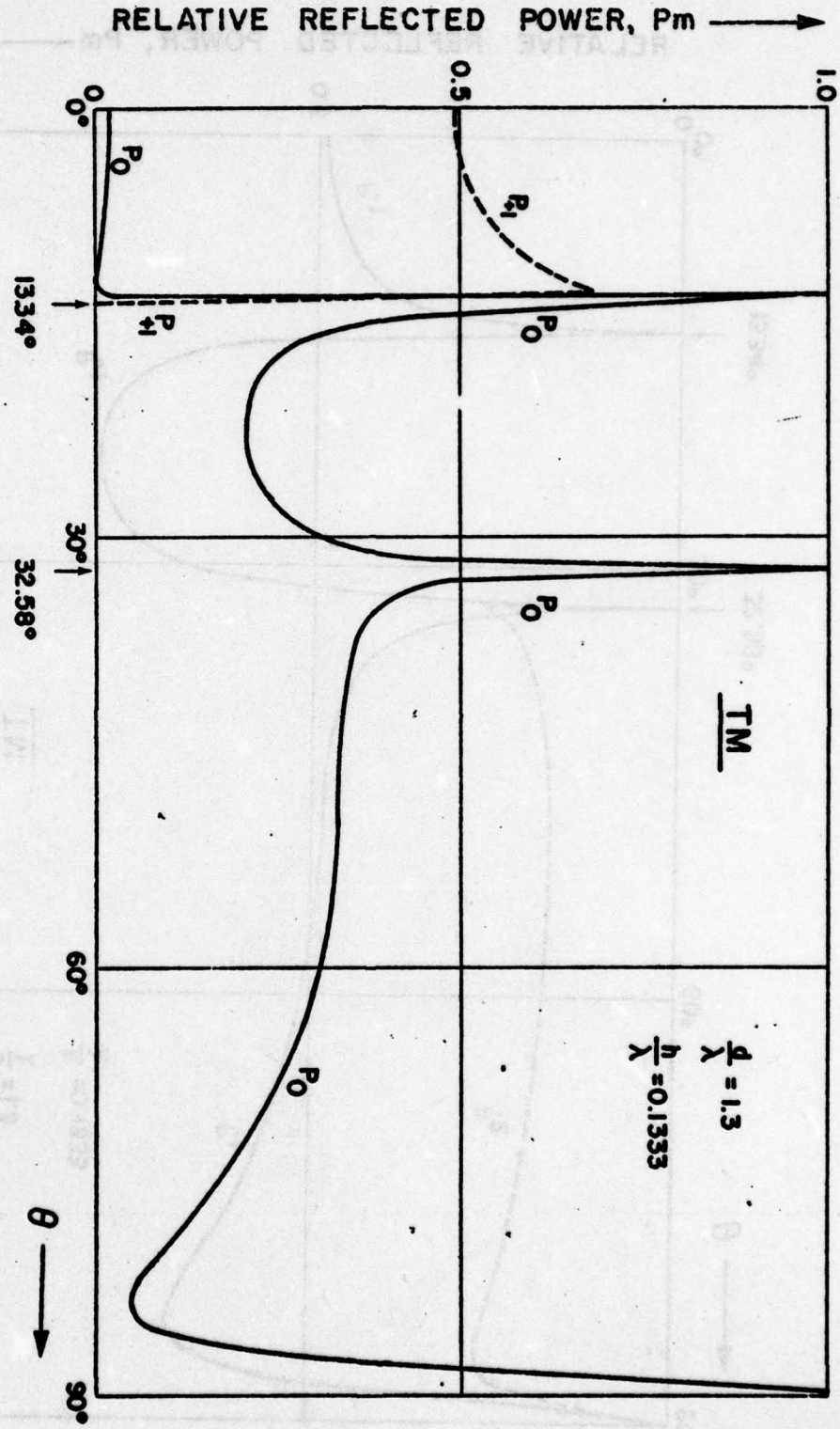

Fig. 15a. Powers P_m of propagating space harmonics vs. incidence angle θ of primary wave. Spectral orders: m = +1, 0. Polarization: TM. Surface parameters: $d/\lambda = 1.3$, $h/\lambda = 0.1333$.

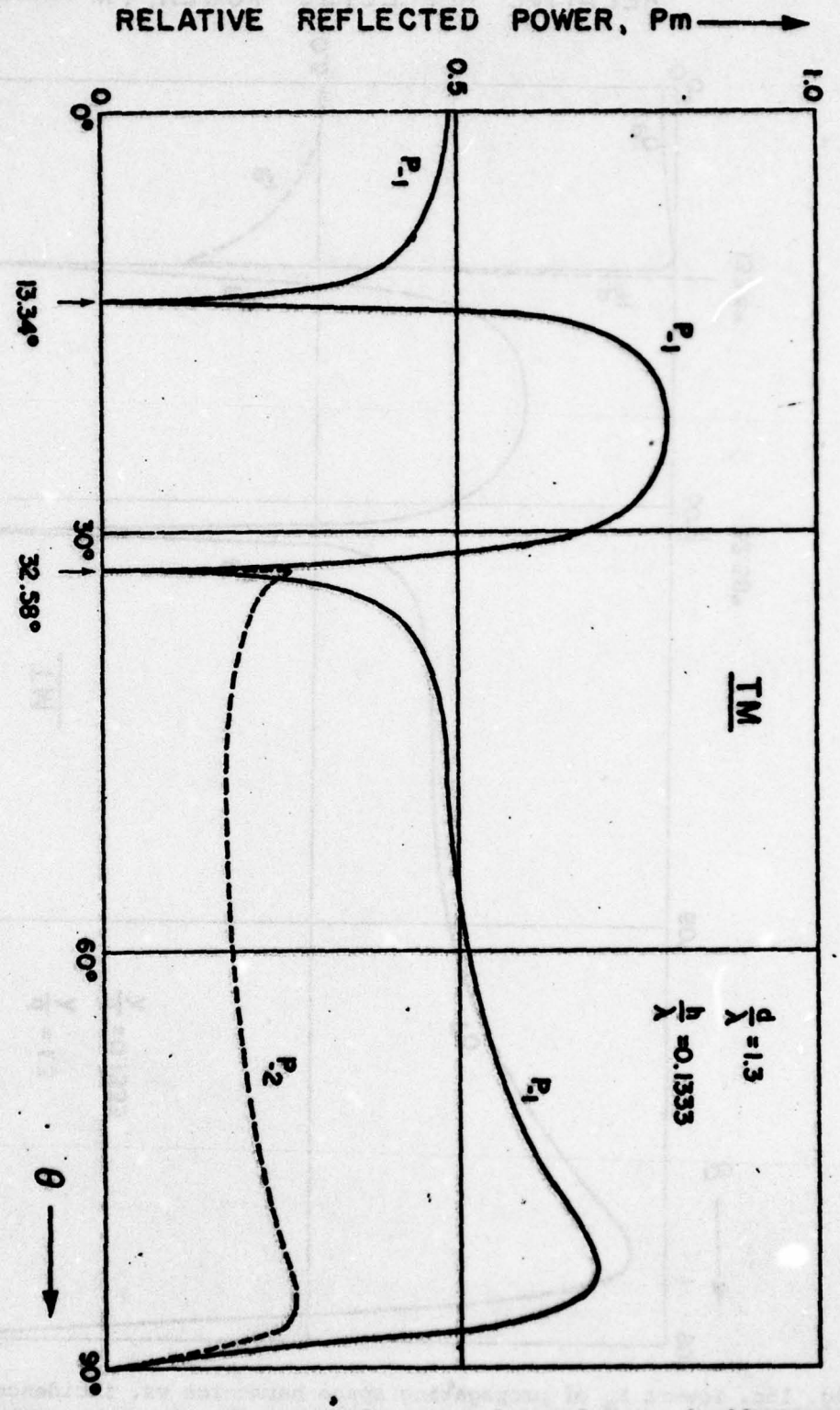

Fig. 15b. Powers P_m of propagating space harmonics vs. incidence angle θ of primary wave. Spectral orders: m = -1,-2. Polarization: TM. Surface parameters: $d/\lambda = 1.3$, $h/\lambda = 0.1333$.

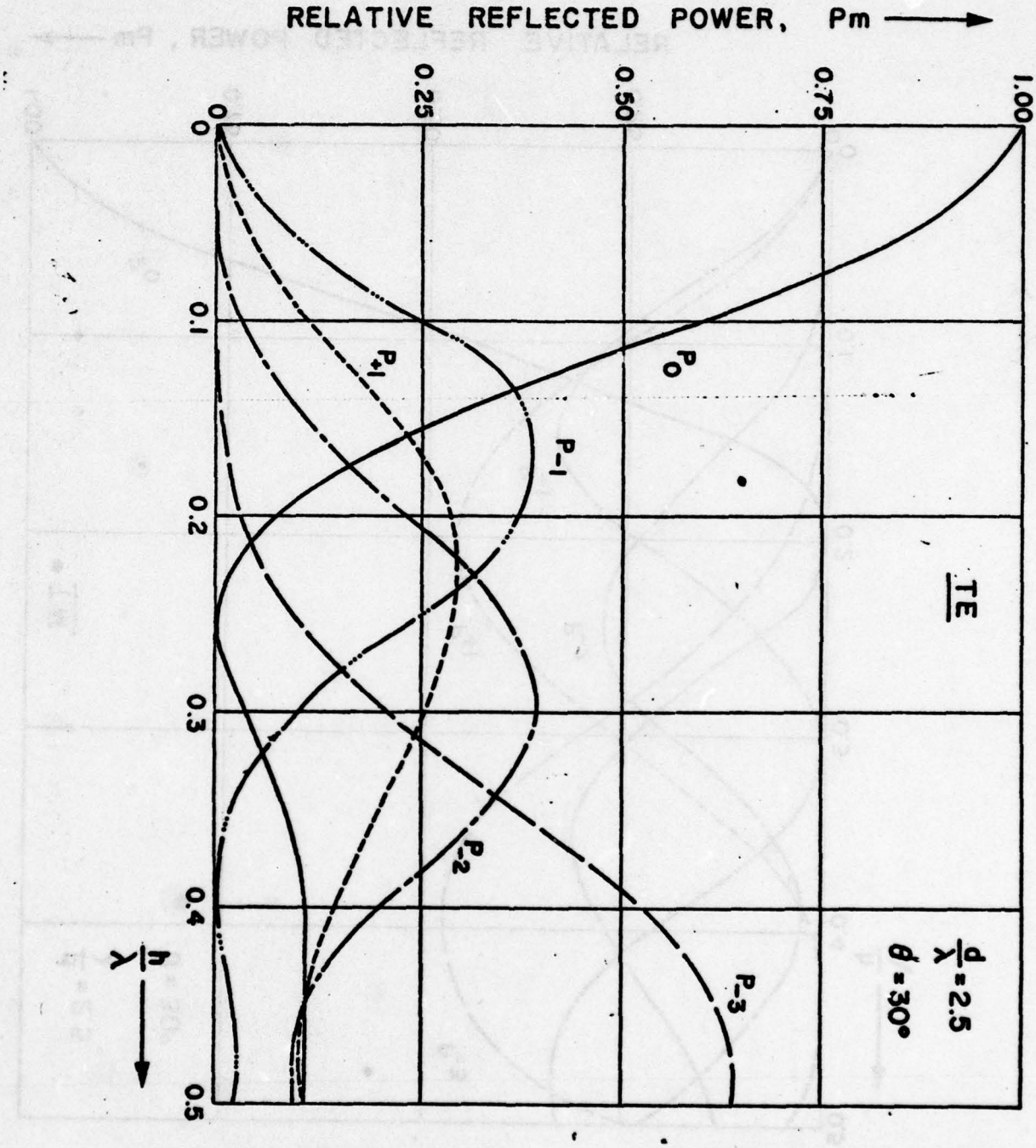

Fig. 16a. Powers P_m of propagating space harmonics as function of groove depth h/λ (TE-polarization, $\theta=30^{\circ}$, $d/\lambda = 2.5$).

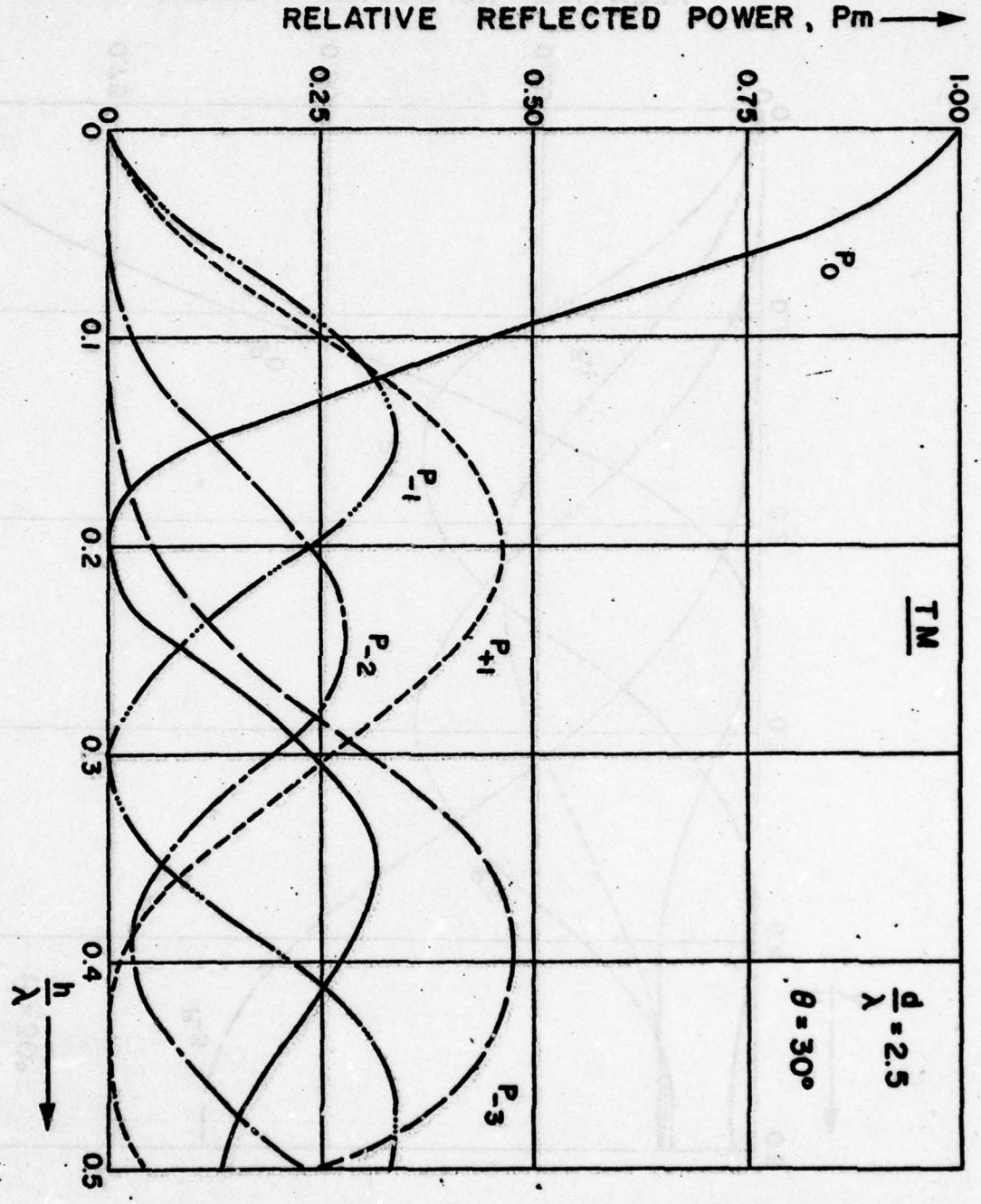

Fig. 16b. Powers P_m of propagating space harmonics as function of groove depth h/λ (TM-polarisation, $\theta = 30^{\circ}$, $d/\lambda = 2.5$).

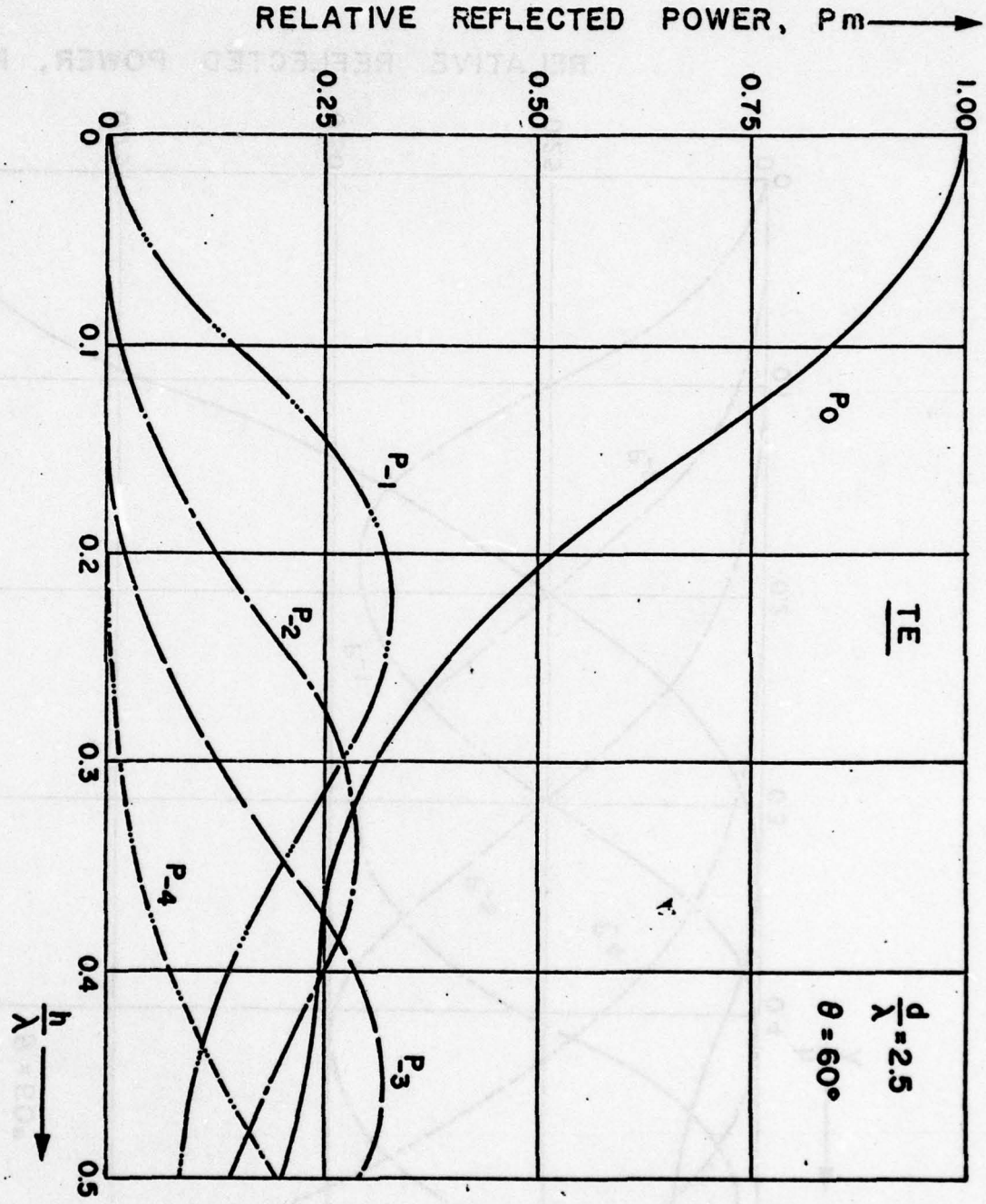

Fig. 17a. Powers P_m of propagating space harmonics as function of groove depth h/λ (TE-polarization, $\theta = 60^\circ$, $d/\lambda = 2.5$).

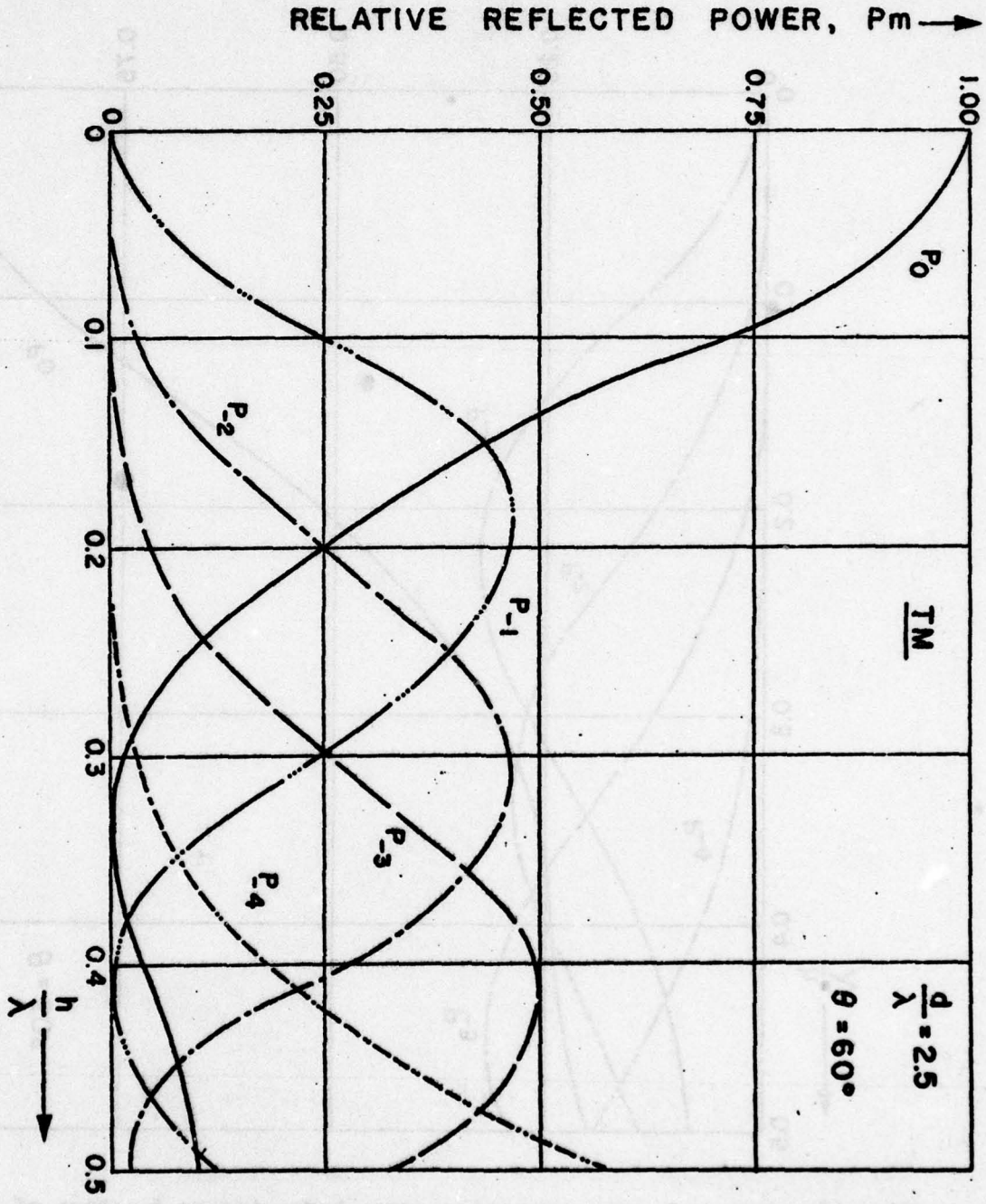

Fig. 17b. Powers P_m of propagating space harmonics vs. function of groove depth h/λ (TM-polarization, $\theta = 60^{\circ}$, $d/\lambda = 2.5$).

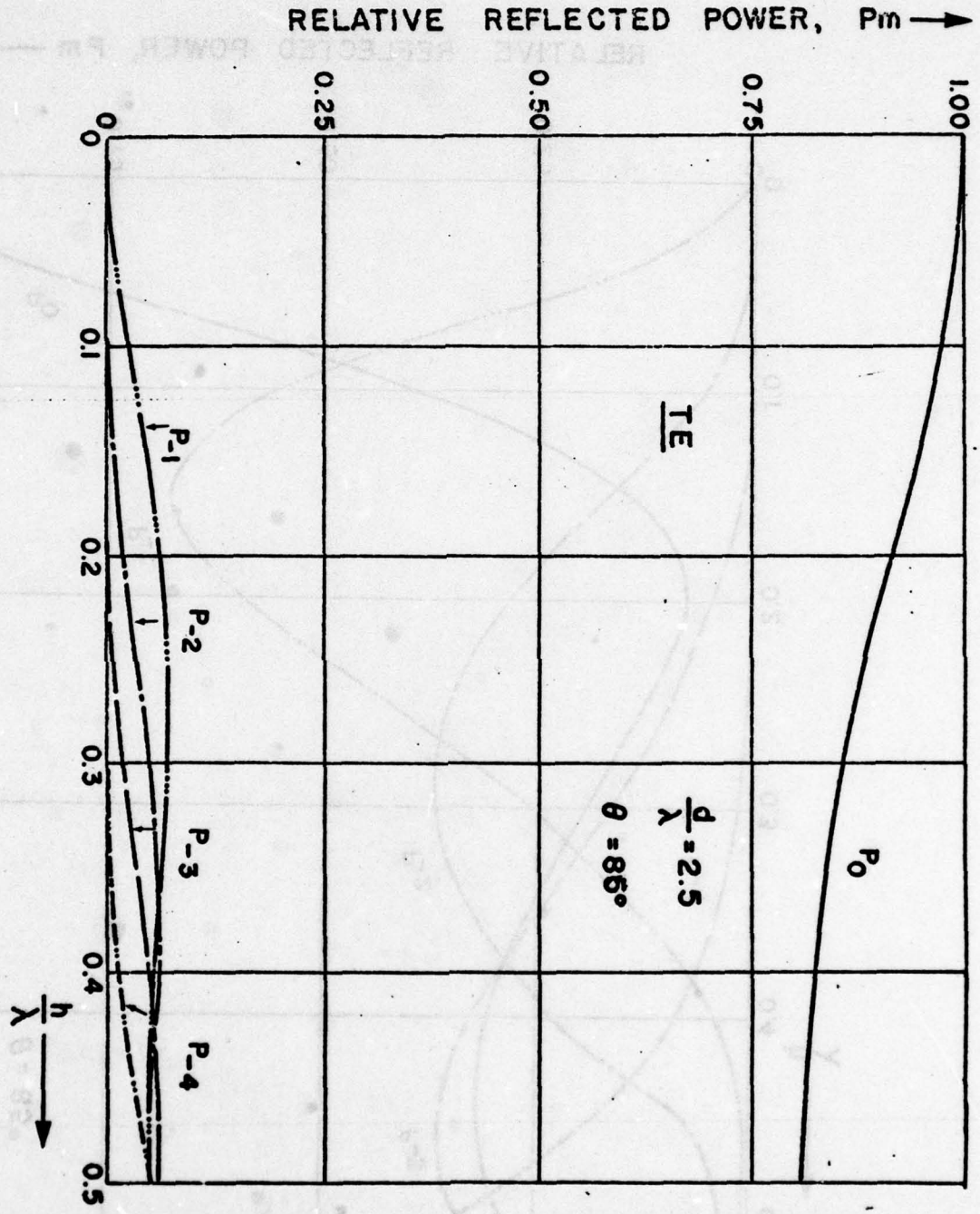

Fig. 18a. Powers P_m of propagating space harmonics vs. function of groove depth h/λ (TE-polarization, $\theta = 85^\circ$, $d/\lambda = 2.5$).

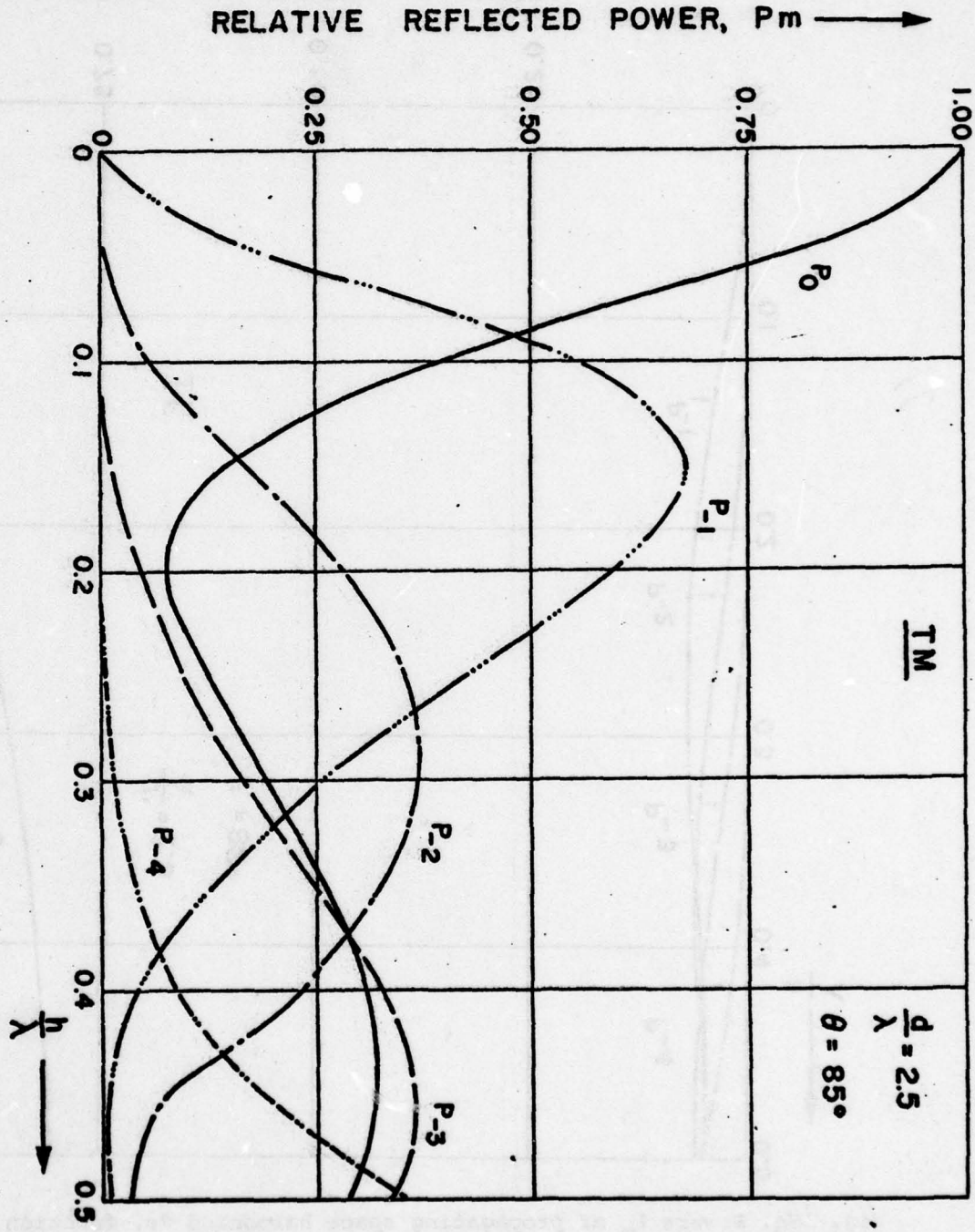

Fig. 18b. Powers P_m of propagating space harmonics vs. function of groove depth h/λ (TE-polarization, $\theta = 85^\circ$, $d/\lambda = 2.5$).

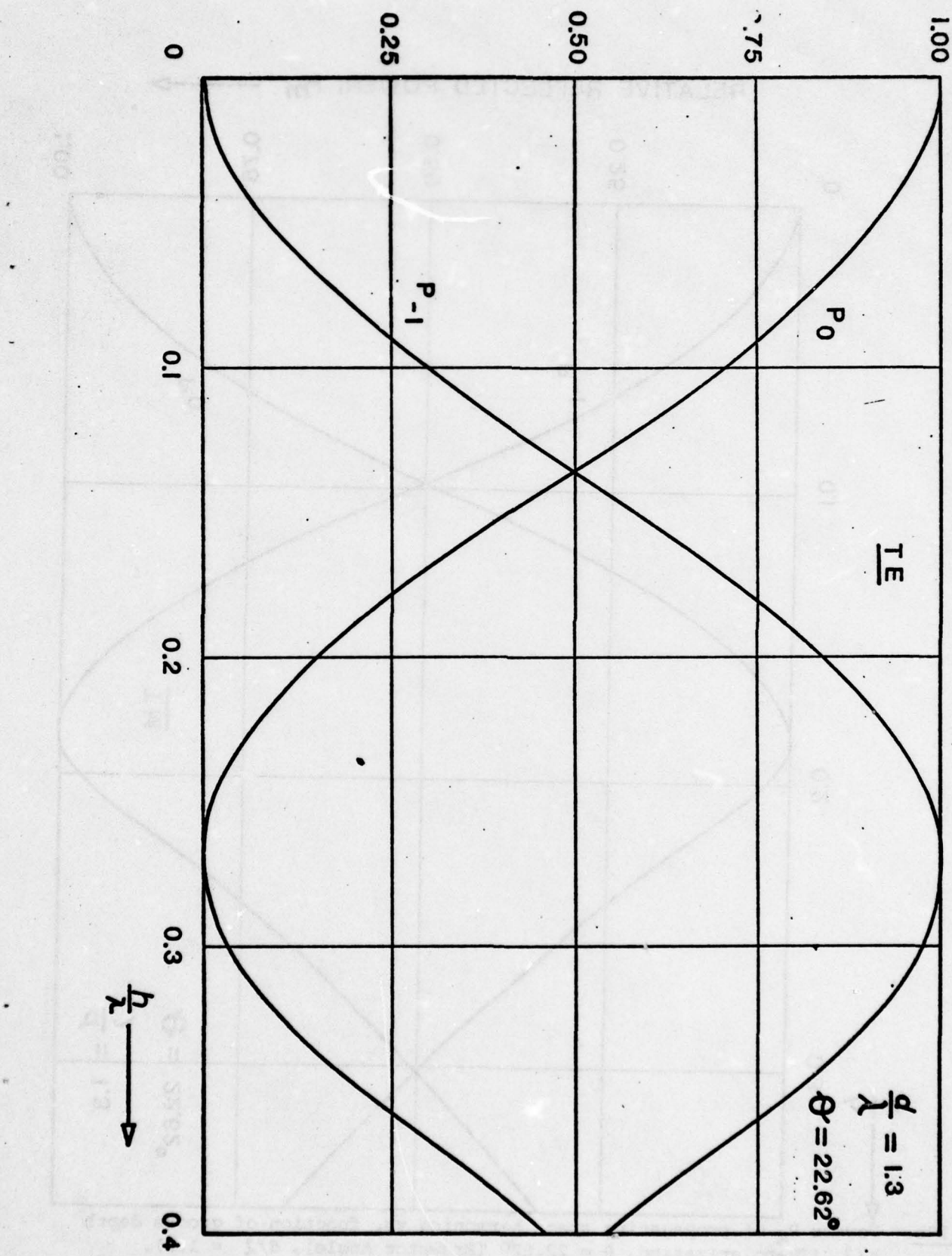

Fig. 19a. Powers P_m of propagating space harmonics as function of groove depth h/λ (TE-polarization, $\theta = 22.62°$ (Brewster Angle), $d/\lambda = 1.3$).

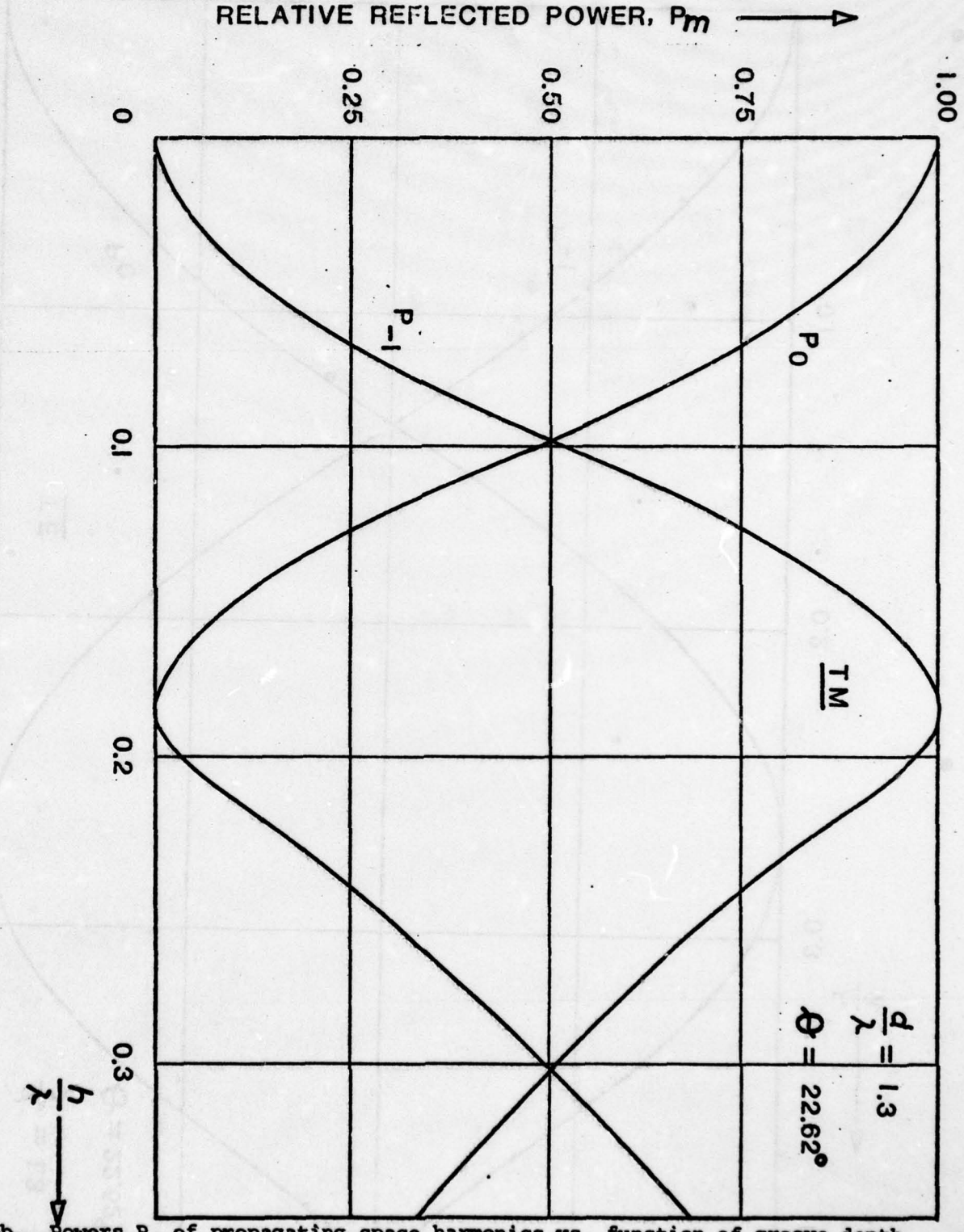

Fig. 19b. Powers P_m of propagating space harmonics vs. function of groove depth h/λ (TM-polarization, $\theta = 22.62^\circ$ (Brewster Angle), $d/\lambda = 1.3$).

TABLE I

Accuracy check using power criterion. Surface parameters: $d/\lambda = 2.5$, $h/\lambda = 0.375$. In addition to power errors ε_{TE} and ε_{TM}, table shows peak amplitudes of current distribution. Near Rayleigh wavelength angles ($\theta_A = 11.54^\circ$ and 36.87°), increments in θ are reduced to 0.5° to make effects of anomalies apparent.

	TE-Polarization		TM-Polarization	
θ	ε_{TE} (%)	$\lvert K_y \rvert_{max}$	ε_{TM} (%)	$\lvert K_t \rvert_{max}$
0	+0.05	2.58	+ 0.44	3.78
10°	-0.12	2.79	- 1.84	4.529
11°	-0.04	2.84	- 1.16	5.30
11.5°	+0.09	2.92	+ 0.40	6.30
12°	-0.35	3.77	- 3.29	5.70
12.5°	-0.27	3.86	- 3.02	5.03
20°	+0.19	3.68	- 0.31	3.87
30°	+0.24	2.83	+ 0.02	3.43
36°	-0.15	2.96	- 0.39	3.61
36.5°	-0.14	3.01	- 0.53	3.60
37°	-2.04	24.97	-+0.47	21.08
37.5°	-1.83	22.60	- 9.05	20.07
38°	-1.69	20.82	- 8.18	19.10
40°	-1.16	17.29	- 6.32	15.63
50°	+0.41	8.75	- 2.66	6.48
60°	+0.58	4.67	- 0.83	3.34
70°	+0.57	2.32	+ 0.04	2.27
80°	+0.17	1.10	+ 0.17	1.48
85°	+0.06	0.92	+ 0.38	0.93

TABLE 2

Accuracy check using power criterion. Surface parameters $d/\lambda = 1.3$, $h/\lambda = 0.1333$. In addition to power errors ε_{TE} and ε_{TM}, table shows peak amplitudes of current distribution. Near Rayleigh wavelength angles ($\theta_A = 13.34^\circ$ and 32.58°), increments in θ are reduced to 0.5° to make effects of anomalies apparent.

	TE-Polarization		TM-Polarization	
θ	ε_{TE} (%)	$\lvert K_y \rvert_{max}$	ε_{TM} (%)	$\lvert K_t \rvert_{max}$
0°	3.10^{-5}	2.06	-4.10^{-6}	2.74
10°	2.10^{-5}	2.06	-4.10^{-5}	3.11
12.5°	2.10^{-5}	2.49	-10^{-4}	3.83
13°	2.10^{-5}	2.54	-2.10^{-4}	4.40
13.5°	10^{-4}	2.63	4.10^{-3}	6.60
14°	10^{-4}	2.62	2.10^{-3}	5.65
14.5°	10^{-4}	2.62	2.10^{-3}	5.20
20°	10^{-4}	2.58	3.10^{-4}	3.74
30°	10^{-4}	2.48	4.10^{-4}	3.60
32°	10^{-4}	2.42	10^{-3}	4.40
32.5°	10^{-4}	2.39	10^{-3}	4.80
33°	5.10^{-4}	2.39	2.10^{-4}	3.48
33.5°	5.10^{-4}	2.40	2.10^{-4}	3.28
34°	5.10^{-4}	2.39	2.10^{-4}	3.17
40°	5.10^{-4}	2.32	3.10^{-4}	2.76
50°	4.10^{-4}	2.06	4.10^{-5}	2.51
60°	2.10^{-4}	1.67	-2.10^{-4}	2.35
70°	10^{-4}	1.18	-4.10^{-4}	2.16
80°	5.10^{-5}	0.62	-5.10^{-4}	1.76
85°	2.10^{-5}	0.31	-4.10^{-4}	1.27

TABLE 3

Accuracy Check using Reciprocity Criterion.
Surface Parameters: $d/\lambda = 2.5$, $h/\lambda = 0.375$
Polarization: TE

θ^a	m	$\theta_m^a = -\theta^i$	$\lvert E_m^{(i)}\rvert^a \cos\theta_m^a$	$\phi_m^a = \arg(E_m^{(s)})^a$	θ^b	m	$\theta_m^b = -\theta^a$	$\lvert E_m^{(i)}\rvert^b \cos\theta_m^b$	$\phi_m^b = \arg(E_m^{(i)})^b$	Error (%)	$\phi_m^a - \phi_m^b$
0.0	-2	-53.13	0.4339	-154.34	+53.13	-2	0.00	0.4328	-154.15	0.25	-0.19
	-1	-23.58	0.2153	+ 34.78	+23.58	-1	0.00	0.2140	+ 34.68	0.61	0.10
	0	0.00	0.5203	- 28.88	0.00	0	0.00	0.5203	- 28.88	0.00	0.00
	+1	+23.58	0.2153	-145.22	-23.58	+1	0.00	0.2140	-145.32	0.61	0.10
	+2	+53.13	0.4339	-154.34	-53.13	+2	0.00	0.4328	-154.15	0.25	-0.19
30	-3	-44.43	0.5265	-170.86	44.43	-3	-30.00	0.5279	-170.65	-0.27	0.21
	-2	-17.46	0.4720	167.38	17.46	-2	-30.00	0.4729	167.19	-0.19	0.19
	-1	5.74	0.0618	107.63	- 5.74	-1	-30.00	0.0639	107.21	-3.25	0.42
	0	30.00	0.2808	40.75	-30.00	0	-30.00	0.2808	40.75	0.0	0.00
	1	64.16	0.2534	49.25	-64.16	1	-30.00	0.2532	49.90	0.08	-0.65
60	-4	-47.22	0.1295	-177.76	47.22	-4	-60.00	0.1296	-177.65	0.08	0.11
	-3	-19.51	0.3434	-171.83	19.51	-3	-60.00	0.3439	-171.86	-0.15	-0.03
	-2	3.79	0.3692	-154.53	- 3.79	-2	-60.00	0.3704	-154.53	-0.32	0.00
	-1	27.78	0.2724	-127.32	-27.78	-1	-60.01	0.2723	-128.06	0.04	-0.64
	0	60.00	0.2518	-102.83	-60.00	0	-60.00	0.2518	-102.83	0.00	0.00
85	-4	-37.14	0.0263	160.36	37.14	-4	-85.03	0.0262	160.26	0.38	0.10
	-3	-11.76	0.0599	169.36	11.76	-3	-85.00	0.0601	169.47	-0.33	-0.11
	-2	11.31	0.0710	-175.13	-11.31	-2	-84.95	0.0723	-175.26	-1.80	-0.13
	-1	36.60	0.0636	-153.07	-36.60	-1	-85.02	0.0634	-153.46	0.32	-0.39
	0	85.00	0.0794	-166.76	-85.00	0	-85.00	0.0794	-166.76	0.00	0.00

$$\text{Error } (\%) = \frac{\lvert E_m^{(i)}\rvert^a \cos\theta_m^a - \lvert E_m^{(i)}\rvert^b \cos\theta_m^b}{\lvert E_m^{(i)}\rvert^b \cos\theta_m^b} \times 100$$

All angles and phases are in degrees

TABLE 4

Accuracy Check using Reciprocy Criterion.
Surface Parameters: $d/\lambda = 2.5$, $h/\lambda = 0.375$
Polarization: TM

θ^a	m	$\theta_m^a = -\theta^b$	$\lvert H_m^{(1)a}\rvert \cos\theta_m^a$	$\psi_m^a = \arg(H_m^{(1)a})$	θ^b	m	$\theta_m^b = -\theta^a$	$\lvert H_m^{(1)b}\rvert \cos\theta_m^b$	$\psi_m^b = \arg(H_m^{(1)b})$	Error (%)	$\psi_m^a - \psi_m^b$
0.00	-2	-53.13	0.4319	- .6909	+53.13	-2	0.00	0.4409	-5.79	-2.04	-0.30
	-1	-23.58	0.3653	+163.18	+23.58	-1	0.00	0.3644	+163.99	0.25	-0.81
	0	0.00	0.2870	- 39.10	0.00	0	0.00	0.2870	- 39.10	0.0	0.0
	+1	+23.58	0.3653	- 16.82	-23.58	+1	0.00	0.3644	- 16.01	0.25	-0.81
	+2	+53.13	0.4319	- 6.09	-53.13	+2	0.00	0.4409	- 5.79	-2.04	-0.30
30	-3	-44.43	0.5417	- 8.38	44.43	-3	-30.000	0.5526	- 8.97	-1.97	-0.59
	-2	-17.46	0.1617	45.02	17.46	-2	-30.00	001589	46.19	5.76	-1.17
	-1	5.74	0.3357	-159.41	- 5.74	-1	-30.00	0.3380	-159.12	-0.68	-0.29
	0	30.00	0.4819	172.10	-30.00	0	-30.00	0.4819	172.10	0.00	0.00
	1	64.16	001418	-179.87	-64.16	1	-30.00	0.1409	179.57	0.64	0.30
60	-4	-47.22	0.2037	- 0.04	47.22	-4	-60.00	0.2051	- 0.05	-0.68	-0.01
	-3	-19.51	0.4656	- 1.92	19.51	-3	-60.00	0.4650	- 2.34	0.13	-0.42
	-2	3.79	0.4289	- 1.29	- 3.79	-2	-60.01	0.4269	- 1.36	0.47	-0.07
	-1	27.78	0.1301	- 7.07	-27.78	-1	-60.01	0.1290	- 6.13	0.85	0.94
	0	60.00	0.0693	171.72	-60.00	0	-60.00	0.0693	171.72	0.00	0.00
85	-4	-37.14	0.0659	- 18.93	37.14	-4	-85.03	0.0670	- 19.95	-1.64	-1.02
	-3	-11.76	0.1566	- 16.84	11.76	-3	-85.00	0.1574	- 17.35	-0.51	-0.51
	-2	11.36	0.1556	- 17.52	-11.31	-2	-84.95	0.1579	- 19.16	-1.46	1.64
	-1	36.60	0.0742	- 12.09	-36.60	-1	-85.02	0.0763	- 12.15	-2.75	-0.06
	0	85.00	0.0465	-168.44	-85.00	0	-85.00	0.0465	-168.44	0.00	0.00

$$\text{Error } (\%) = \frac{\lvert H_m^{(1)a}\rvert \cos\theta_m^a - \lvert H_m^{(1)b}\rvert \cos\theta_m^b}{\lvert H_m^{(1)b}\rvert \cos\theta_m^b} \times 100$$

All angles and phases are in degrees

TABLE 5

Dependence of Power Errors ϵ_{TE} and ϵ_{TM} on Surface Depth.
Surface Period: $d/\lambda = 2.5$
Incidence Angle: $\theta = 30^{\circ}$

$\frac{h}{\lambda}$	ϵ_{TE} (%)	ϵ_{TM} (%)
0.05	$1.0 \cdot 10^{-7}$	$-2.6 \cdot 10^{-7}$
0.1	$1.6 \cdot 10^{-6}$	$-2.8 \cdot 10^{-6}$
0.15	$5.0 \cdot 10^{-4}$	$-3.9 \cdot 10^{-3}$
0.2	$-3.4 \cdot 10^{-2}$	$-4.8 \cdot 10^{-2}$
0.25	$3.7 \cdot 10^{-2}$	$-1.5 \cdot 10^{-1}$
0.3	$8.7 \cdot 10^{-2}$	$-2.0 \cdot 10^{-1}$
0.35	$1.7 \cdot 10^{-1}$	$1.4 \cdot 10^{-1}$
0.4	$4.5 \cdot 10^{-1}$	$7.8 \cdot 10^{-2}$
0.45	1.59	-5.01
0.5	1.27	-2.77

TABLE 6

Dependence of Power Errors ϵ_{TE} and ϵ_{TM} on Surface Depth.
Surface Period: $d/\lambda = 1.3$
Incidence Angle: $\theta = 22.62^\circ$ (Brewster Angle)

$\frac{h}{\lambda}$	ϵ_{TE} (%)	ϵ_{TM} (%)
0.05	$2 \cdot 10^{-5}$	$4 \cdot 10^{-5}$
0.1	$7 \cdot 10^{-5}$	$1.5 \cdot 10^{-4}$
0.15	$1.5 \cdot 10^{-4}$	$3.2 \cdot 10^{-4}$
0.2	$-3.0 \cdot 10^{-4}$	$1.0 \cdot 10^{-2}$
0.25	$1.1 \cdot 10^{-2}$	$2.5 \cdot 10^{-1}$
0.3	-1.29	5.26
0.35	-9.53	45.32
0.4	2.72	-17.97

TABLE 7a

Comparison of approaches: Complex amplitudes of space harmonics. (TE - polarization; $d/\lambda=0.2$, $h/\lambda=0.1$)

	$\theta=0^\circ$		$\theta=30^\circ$		$\theta=60^\circ$	
	Mag.	Phase	Mag.	Phase	Mag.	Phase
	$\lvert E_0^{(1)}\rvert$	$\phi_0^{(1)}$ (°)	$\lvert E_0^{(1)}\rvert$	$\phi_0^{(1)}$ (°)	$\lvert E_0^{(1)}\rvert$	$\phi_0^{(1)}$ (°)
1. Whitman, Schwering	0.9995	+128.76	0.9996	-135.62	0.9999	-154.37
2. Tong, Senior	1.0050	50.81	0.9940	44.33	1.0000	25.90
3. Physical Optics w/o Shadow	0.6425	0	0.7251	0	0.9037	0
4. Physical Optics with Shadow	0.6425	0	0.1253	15.96	0.1770	19.41

TABLE 7b

Comparison of approaches: Complex amplitudes of space harmonics. (TE - polarization; $d/\lambda=1.9$, $h/\lambda=0.25$; $\theta=0^\circ$)

	Mag.	Phase	Mag.	Phase	Mag.	Phase
	$\lvert E_0^{(1)}\rvert$	$\phi_0^{(1)}$ (°)	$\lvert E_{-1}^{(1)}\rvert$	$\phi_{-1}^{(1)}$ (°)	$\lvert E_1^{(1)}\rvert$	$\phi_1^{(1)}$ (°)
1. Whitman, Schwering	0.4919	20.71	0.6677	- 82.02	0.6676	- 81.97
2. Tong, Senior	0.4920	-160.27	0.6630	107.05	0.6630	107.05
3. Physical Optics	0.3042	0	0.4389	90	0.4389	90

$\phi_m^{(1)} \equiv \arg E_m^{(1)}$

TABLE 7c

Comparison of approaches: Complex amplitudes of space harmonics (TE - polarization; d/λ 0.4, h/λ=0.2)

	$\theta=0^\circ$		$\theta=60^\circ$	
	Mag. $\lvert E_0^{(i)} \rvert$	Phase $\phi_0^{(i)}$ (°)	Mag. $\lvert E_0^{(i)} \rvert$	Phase $\phi_0^{(i)}$ (°)
1. Whitman, Schwering	0.9918	-80.83	0.9995	-130.47
2. Togg, Senior	0.9998	-80.81	1.0230	49.89
3. Physical Optics w/o Shadow	0.0549	0	0.6450	0
4. Physical Optics with Shadow	0.0549	0	0.4750	60.37

TABLE 7d

Comparison of approaches: Complex amplitudes of space harmonics (TE - polarization; d/λ=0.2, h/λ=0.03; $\theta=0^\circ$)

	Mag. $\lvert E_0^{(i)} \rvert$	Phase $\phi_0^{(i)}$ (°)	
1. Whitman, Schwering	1.0000	-171.59	
2. Tong, Senior	1.0000	8.12	
3. Physical Optics	0.9647	0	

TABLE 8a

Comparison of approaches: Complex amplitudes of space harmonics. (TM - polarization; $d/\lambda=0.2$, $h/\lambda=0.1$)

	$\theta=0^\circ$		$\theta=30^\circ$		$\theta=60^\circ$	
	Mag. $\lvert H_0^{(i)}\rvert$	Phase $\psi_0^{(i)}$ (°)	Mag. $\lvert H_0^{(i)}\rvert$	Phase $\psi_0^{(i)}$ (°)	Mag. $\lvert H_0^{(i)}\rvert$	Phase $\psi_0^{(i)}$ (°)
1. Whitman, Schwering	0.9978	-12.10	0.9982	-26.88	0.9994	-77.39
2. Tong, Senior	0.9830	-12.45	0.9910	-23.82	1.0640	-67.24
3. Physical Optics w/o Shadow	0.6425	0	0.7251	0	0.9037	0
4. Physical Optics w/Shadow	0.6425	0	0.1550	-65.17	0.5440	-166.31

TABLE 8b

Comparison of approaches: Complex amplitudes of space harmonics. (TM - polarization; $d/\lambda=1.9$, $h/\lambda=0.25$; $\theta=0^\circ$)

	Mag. $\lvert H_0^{(i)}\rvert$	Phase $\psi_0^{(i)}$ (°)	Mag. $\lvert H_{-1}^{(i)}\rvert$	Phase $\psi_{-1}^{(i)}$ (°)	Mag. $\lvert H_1^{(i)}\rvert$	Phase $\psi_1^{(i)}$ (°)
1. Whitman, Schwering	0.9008	99.39	0.3320	+51.93	0.3347	+52.52
2. Tong, Senior	0.9040	-80.50	0.3350	52.55	0.3350	52.55
3. Physical Optics	0.3042	0	0.4389	90	0.4389	90

$\psi_m^{(i)} \equiv \arg H_m^{(i)}$

TABLE 8c

Comparison of approaches: Complex amplitudes of space harmonica (TM - polarization; $d/\lambda = 0.4$, $h/\lambda = 0.2$)

	$\theta = 0°$		$\theta = 60°$	
	Mag $\lvert H_0^{(1)} \rvert$	Phase $\psi_0^{(1)}$ (°)	Mag $\lvert H_0^{(1)} \rvert$	Phase $\psi_0^{(1)}$ (°)
1. Whitman, Schwering	1.0113	-109.32	0.9969	-152.11
2. Tong, Senior	0.9350	-107.19	1.0140	-145.28
3. Physical Optic w/o shadow	0.0549	0	0.6450	0
4. Physical Optics with shadow	0.0549	0	0.1290	-131.32

TABLE 8d

Comparison of approaches: Complex amplitudes of space harmonics (TM - polarization: $d/\lambda = 0.2$, $h/\lambda = 0.03$; $\theta = 0°$)

	Mag $\lvert H_0^{(1)} \rvert$	Phase $\psi_0^{(1)}$ (°)
1. Whitman, Schwering	1.0000	-0.50
2. Tong, Senior	0.9986	-0.55
3. Physical Optics	0.9988	0

TABLE 9

Comparison of approaches: Total scatter power and relative power error (TE - polarization)

			Whitman, Schwering		Tong, Senior		Physical Optics w/o Shadow		Physical Optics with Shadow	
d/λ	h/λ	θ (°)	Power *	ε_{TE} (%)	Power	ε_{TE} (%)	Power	ε_{TE} (%)	Power	ε_{TE} (%)
0.2	0.1	0	0.9989	-0.11	0.9970	-0.30	0.4128!	-58.72	0.4128	-58.72
0.2	0.1	30	0.9993	-0.07	0.9889	-1.18	0.5258	-47.50	0.5860	-41.45
0.2	0.1	60	0.9998	-0.02	1.0026	0.26	0.8168	-18.32	1.2344	23.44
0.2	0.01	0	1.0000	0.00	0.9990	-0.10	0.9921	- 0.79	0.9921	- 0.79
0.2	0.03	0	1.0000	0.00	1.0042	0.42	0.9308	- 6.92	0.9308	- 6.92
0.4	0.2	0	0.9836	-1.64	0.9976	-0.76	0.0030	-99.70	0.0030	-99.70
0.4	0.2	60	0.9990	-0.10	1.0136	1.36	0.4120	-58.78	0.2294	-76.47
1.9	0.25	0	1.0000	0.00	0.9996	0.04	0.4202	-57.98	0.4202	-57.98

*Power (normalized) = $\sum_m P_m = \frac{\sum_m |E_m^{(i)}|^2 \cos\theta_m}{\cos\theta}$

TABLE 10

Comparison of approaches: Total scatter power and relative power error (TM - polarization)

			Whitman, Schwering		Tong, Senior		Physical Optics w/o Shadow		Physical Optics with Shadow	
d/λ	h/λ	θ (°)	Power *	ε_{TM} (%)	Power	ε_{TM} (%)	Power	ε_{TM} (%)	Power	ε_{TM} (%)
0.2	0.1	0	0.9957	-0.43	0.9848	-1.52	0.4728	-58.72	0.4728	-58.72
0.2	0.1	30	0.9964	-0.36	0.9852	-1.43	0.5259	-47.30	0.0240	-98.00
0.2	0.1	60	0.9998	-0.12	1.0150	1.50	0.8166	-18.34	0.2958	-70.42
0.2	0.01	0	1.0000	0.00	0.9980	-0.20	0.9921	- 0.79	0.9921	- 0.79
0.2	0.03	0	1.0000	0.00	0.9987	-0.13	0.9308	- 6.92	0.9308	- 6.92
0.4	0.2	0	1.0226	2.26	0.9823	-1.77	0.0030	-99.70	0.0030	-99.70
0.4	0.2	60	0.9938	-0.62	0.5042	0.84	0.4122	-58.78	0.0160	-98.50
1.9	0.25	0	1.0004	0.04	0.9974	-0.26	0.4202	-57.98	0.4202	-57.98

*Power (normalized) = $\sum_m P_m = \dfrac{\sum_m |H_m^{(1)}|^2 \cos\theta_m}{\cos\theta}$

TABLE IIa

Scattering from surfaces of large surface period: Comparison of W-S theory and physical optics approximation.
Surface parameters: $d/\lambda=10$, $h/\lambda=0.5$
Angle of incidence: $\theta=15^{\circ}$.

Spectral Order m	Power P_m of Space Harmonics		
	W-S Theory		PO Approximation w/o shadow
	TE	TM	
-12	P_m= 0.00	0.00	0.00
-11			
- 7	0.017	0.018	0.018
- 6	0.071	0.073	0.072
- 5	0.152	0.153	0.153
- 4	0.126	0.122	0.124
- 3	0.005	0.004	0.004
- 2	0.075	0.077	0.076
- 1	0.064	0.060	0.062
0	0.027	0.030	0.029
+ 1	0.083	0.079	0.081
+ 2	0.041	0.045	0.043
+ 3	0.054	0.048	0.051
+ 4	0.180	0.179	0.180
+ 5	0.090	0.094	0.092
+ 6	0.013	0.015	0.014
+ 7	0.00	0.00	0.00
$\sum_m P_m$:	1.000	1.000	1.000
$\lvert\varepsilon_{TE}\rvert, \lvert\varepsilon_{TM}\rvert$:	$6.5\cdot10^{-4}$ %	$2.6\cdot10^{-4}$ %	$1.6\cdot10^{-2}$ %

TABLE 11b

Scattering from surfaces of large surface period: Comparison of W-S theory and physical optics approximation.
Surface parameters: $d/\lambda=10$, $h/\lambda=0.5$
Angle of incidence: $\theta=45^{\circ}$

Spectral Order m	Power P_m of Space Harmonics		
	W-S Theory		PO Approximation w/o Shadow
	TE	TM	
-17	P_m= 0.00	0.00	0.00
-16			
- 7	0.008	0.009	0.008
- 6	0.036	0.038	0.037
- 5	0.106	0.110	0.108
- 4	0.182	0.182	0.182
- 3	0.138	0.128	0.132
- 2	0.008	0.005	0.005
- 1	0.070	0.096	0.081
0	0.100	0.145	0.111
+ 1	0.018	0.061	0.009
+ 2	0.333	0.225	0.233
$\sum_m P_m$:	1.000	1.000	0.908
$\lvert\varepsilon_{TE}\rvert, \lvert\varepsilon_{TM}\rvert$:	$1.5\cdot10^{-4}$ %	$1.9\cdot10^{-3}$ %	9.2 %

TABLE 11c:

Scattering from surfaces of large surface period:
Comparison of W-S theory and physical optics approximation
Surface parameters: $d/\lambda = 10$, $h/\lambda = 0.5$
Angle of incidence: $\theta = 75^\circ$

Spectral Order m	Power P_m of Space Harmonics				
	W - S Theory		P O Approximation		
			With Shadow		Without Shadow
	TE	TM	TE	TM	TE & TM
-19	P_m=0.00	0.00	0.00	0.00	0.00
-18					
-6	0.002	0.003	0.003	0.015	0.003
-5	0.012	0.019	0.017	0.014	0.016
-4	0.044	0.075	0.060	0.058	0.064
-3	0.120	0.201	0.178	0.181	0.175
-2	0.219	0.338	0.323	0.370	0.310
-1	0.264	0.297	0.290	0.405	0.316
00	0.339	0.067	0.206	0.024	0.194
$\sum_m P_m$:	1.000	1.000	1.077	1.074	1.077
$\lvert\epsilon_{TE}\rvert, \lvert\epsilon_{TM}\rvert$:	$5.3 \cdot 10^{-4}$ %	$3.4 \cdot 10^{-4}$ %	7.74%	7.41%	7.74%

TABLE IId

Scattering from surfaces of large surface period:
Comparison of W-S theory and physical optics approximation.
Surface parameters: $d/\lambda=10$, $h/\lambda=0.5$
Angle of incidence: $\theta=85^\circ$

Spectral Order m	Power P_m of Space Harmonics				
	W - S Theory		P O Approximation		
			With Shadow		Without Shadow
	TE	TM	TE	TM	TE & TM
-19	P_m=0.00	0.00	0.00	0.00	0.00
-18					
-10			0.00	0.014	
- 9			0.001	0.016	
- 8			0.002	0.003	
- 7		0.00	0.003	0.031	0.00
- 6	0.00	0.002	0.005	0.055	0.001
- 5	0.003	0.011	0.009	0.029	0.009
- 4	0.011	0.052	0.020	0.066	0.046
- 3	0.035	0.166	0.088	0.234	0.166
- 2	0.077	0.338	0.135	0.341	0.406
- 1	0.124	0.379	0.191	0.218	0.647
0	0.750	0.053	0.960	0.117	0.858
$\sum_m P_m$:	1.000	1.000	1.463	1.155	2.133
$\lvert\varepsilon_{TE}\rvert$ $\lvert\varepsilon_{TM}\rvert$:	$1.5\cdot10^{-6}$%	$1.3\cdot10^{-2}$%	46.3%	15.5%	113.4%